Mitochondrial outer membrane integrity regulates a ubiquitin-dependent NF-κB inflammatory response

Esmee Vringer [1,2], Joel S Riley [1,2,3], Annabel Black [1,2], Catherine Cloix [1,2], Sergio Lilla [2], Henning Walczak [4,5,6], Mads Gyrd-Hansen [7], Danny T Huang [1,2], Sara Zanivan [1,2], Stephen WG Tait [1,2 *]

[1] School of Cancer Sciences, University of Glasgow, Switchback Road, Glasgow, G61 1BD, UK.

[2] Cancer Research UK Beatson Institute, Switchback Road, Glasgow, G61 1BD, UK.

[3] Institute of Developmental Immunology, Biocenter, Medical University of Innsbruck, Innsbruck, Austria.

[4] Centre for Cell Death, Cancer, and Inflammation (CCCI), UCL Cancer Institute, University College London, London, UK.

[5] CECAD Cluster of Excellence, University of Cologne, Cologne, Germany.

[6] Center for Biochemistry, Faculty of Medicine and University Hospital Cologne, University of Cologne, Cologne, Germany.

[7] Department of Immunology and Microbiology, LEO Foundation Skin Immunology Research Center, University of Copenhagen, Copenhagen, Denmark.

* Corresponding author: Stephen Tait, e-mail: stephen.tait@glasgow.ac.uk

Abstract

Mitochondria are often essential for apoptosis through mitochondrial outer membrane permeabilization (MOMP). This central event enables cytochrome *c* release leading to caspase activation and rapid cell death. Recently, MOMP has been shown to be inherently pro-inflammatory, for instance, by enabling mitochondrial DNA-dependent activation of cGAS-STING signalling. Alongside having emerging functions in health and disease, MOMP associated inflammation can also elicit anti-tumour immunity. Nonetheless, how MOMP triggers inflammation and how the cell counteracts this remains poorly defined. We find that upon MOMP, mitochondria are ubiquitylated in a promiscuous manner targeting proteins localised to both inner and outer mitochondrial membranes. Mitochondrial ubiquitylation serves to recruit the essential adaptor molecule, NEMO, leading to activation of pro-inflammatory NF-κB signalling. We find that disruption of mitochondrial outer membrane integrity through different means leads to engagement of a similar pro-inflammatory signalling platform. Thus, mitochondrial integrity directly controls inflammation, such that permeabilised mitochondria initiate NF-κB signalling. This event may be important for the various pathophysiological functions of MOMP-associated inflammation.

Introduction

Apoptotic cell death is considered an immunosilent form of cell death, in line with it being the major type of homeostatic cell death. Mitochondrial outer membrane permeabilization (MOMP) is often essential to initiate apoptosis by enabling cytochrome *c* release, leading to rapid caspase activation and cell death (Bock & Tait, 2020). Nonetheless, upon a lethal stress, MOMP commits a cell to die regardless of caspase activation through so-called caspase-independent cell death (CICD). This is due to widespread MOMP causing a catastrophic loss in mitochondrial function (Lartigue *et al*, 2009).

Recent research has revealed that MOMP is inherently pro-inflammatory (Giampazolias *et al*, 2017; Marchi *et al*, 2022). For instance, mitochondrial DNA (mtDNA) is released from permeabilised mitochondria through BAX/BAK macropores, leading to activation of cGAS-STING signalling and a type I interferon response (McArthur *et al*, 2018; Riley *et al*, 2018). Importantly, while wholly dispensable for cell death, caspase activity serves to inhibit inflammation during mitochondrial apoptosis. Caspases inhibit inflammation in dying cells through multiple means, including direct cleavage of pro-inflammatory signalling proteins such as cGAS, inhibition of protein translation and promoting rapid removal of dying cells via the exposure of “eat-me” signals (McIlwain *et al*, 2013; Ning *et al*, 2019; Ravichandran, 2011).

By enhancing MOMP-induced inflammation through caspase-inhibition, we and others have shown that engaging CICD in tumour cells can lead to anti-tumour immunity dependent on cGAS-STING and NF-κB signalling in the dying cell (Giampazolias *et al.*, 2017; Han *et al*, 2020). We also reported that MOMP can occur

in a limited cohort of mitochondria – a phenomemon we termed minority MOMP– in the absence of cell death (Cao *et al*, 2022; Ichim *et al*, 2015). Minority MOMP can promote caspase-dependent DNA-damage. Intriguingly others have discovered that minority MOMP causes inflammation required for the restriction of bacteria. (Brokatzky *et al*, 2019). More recently, we have found that minority MOMP contributes to the inflammatory phenotype of senescent cells thereby directly bridging apoptotic signalling with senescence (Chapman et al, Res Square).

Thus, MOMP induced inflammation - alongside having physiological functions - represents a therapeutic target in cancer. Nonetheless, how MOMP elicits inflammation and how this is restrained remain poorly defined. Specifically, how permeabilised mitochondria are targeted for degradation – potentially limiting inflammation following MOMP, is not known. We initially set out to address this question, finding that upon MOMP, mitochondria are promiscuously ubiquitylated. Mitochondrial ubiquitylation has been shown to serve as signal for mitophagy, best evidenced in mitophagy promoted by the E3 ubiquitin ligase Parkin (Vargas *et al*, 2022). Surprisingly, upon MOMP, we find that autophagy is not essential for mitochondrial degradation. Upon further investigation, we found that MOMP-induced ubiquitylation of mitochondria serves as an inflammatory signal, recruiting the essential NF-κB signalling adaptor, NF-κB essential modulator (NEMO). In this way, mitochondrial outer membrane integrity dictates the initiation of an NF-κB inflammatory response, contributing to MOMP-induced inflammation.

Results

Permeabilised mitochondria are ubiquitylated and degraded independent of canonical autophagy

Following MOMP, autophagy targets permeabilised mitochondria for degradation and suppresses MOMP-induced inflammation (Colell *et al*, 2007; Lindqvist *et al*, 2018). Given this, our initial goal was to understand how MOMP triggers mitochondrial removal. To engage mitochondrial apoptosis, U2OS cells were treated a combination of BH3-mimetics, ABT-737 (inhibits BCL-2, BCL-xL and BCL-w) and S63845 (inhibits MCL-1) then analysed for cell viability by SYTOX Green exclusion and Incucyte live-cell imaging. Combined BH3-mimetic treatment in wild-type U2OS cells led to rapid cell death that was inhibited by co-treatment with pan-caspase inhibitor Q-VD-OPh or CRISPR-Cas9 mediated deletion of BAX and BAK, two proteins essential for MOMP, confirming engagement of mitochondrial apoptosis (**Supplemental Figures 1A** and **B**). Using this approach, we next assessed mitochondrial content in U2OS cells following MOMP under conditions of CICD by using the combination treatment of ABT-737, S63845 and Q-VD-OPh. Mitochondrial content was determined by western blot for mitochondrial proteins or via qPCR for mitochondrial DNA (**Figure 1A** and **1B)**. Reduction in cellular mitochondrial content was observed specifically following MOMP, as evidenced by a loss of mtDNA and mitochondrial protein content in a BAX/BAK dependent manner (**Figure 1A** and **1B**). Mitochondrial ubiquitylation is a well-established signal for autophagic removal of mitochondria, a process called mitophagy (Vargas *et al.*, 2022). Therefore, we investigated whether mitochondria are ubiquitylated upon MOMP. SVEC4-10 murine endothelial cells were treated to undergo CICD and mitochondrial-enriched fractions were probed for ubiquitylation by western blot using a pan-ubiquitin antibody.

Consistent with engagement of MOMP, SMAC (also called DIABLO) was depleted from the mitochondrial-enriched fraction upon CICD. Importantly, an extensive increase of protein ubiquitylation was detected in the mitochondria-enriched fraction specifically following MOMP (**Figure 1C**)**.** Increased ubiquitylation was dependent upon MOMP since it was absent in BAX/BAK deficient cells (**Supplemental Figure 1C**). To corroborate these findings, U2OS EMPTY^{CRISPR} and BAX/BAK^{CRISPR} cells were immunostained following induction of CICD using a combination of anti-ubiquitin and mitochondrial COXIV antibodies. Upon CICD, ubiquitin localised with mitochondria in U2OS EMPTY^{CRISPR} cells but not in U2OS BAX/BAK^{CRISPR} cells (**Figure 1D** and **1E**), in line with the earlier mitochondrial fractionation experiment (**Supplemental Figure 1C**). To investigate whether inhibition of caspase activity was required for the ubiquitylation of mitochondria following MOMP, SVEC4-10 cells were treated with BH3-mimetics with or without the pan-caspase inhibitor Q-VD-OPh. Western blot analysis of mitochondria-enriched fractions demonstrated increased ubiquitylation irrespective of caspase inhibition (**Supplemental Figure 1D**).

Ubiquitylation can target organelles for autophagic degradation via recruitment of specific autophagy adaptor molecules (Vargas *et al.*, 2022). Therefore, we investigated whether autophagy was required for degradation of mitochondria following MOMP by engaging CICD in U2OS cells deficient in ATG5 or ATG7, two proteins essential for canonical macroautophagy (Komatsu *et al*, 2005; Kuma *et al*, 2004). ATG5 and ATG7 loss, as well as functional autophagy deficiency, evident by an absence of lipidated LC3, was confirmed via western blot (**Figure 1F**). Surprisingly, treatment of cells with BH3-mimetics and caspase inhibitor led to a reduction of mitochondria (as determined by the loss of mitochondrial protein content) independent of autophagy (**Figure 1F**). These data demonstrate that upon MOMP, mitochondria

143 are ubiquitylated and can be degraded in a manner that does not require canonical
144 autophagy.

145

146 **Widespread mitochondrial protein ubiquitylation occurs upon MOMP**

147 We next characterised mitochondrial protein ubiquitylation upon MOMP. Di-
148 glycine remnant proteomics can identify ubiquitylated proteins by the
149 immunoprecipitation of modification diGly-motifs left on ubiquitylated proteins after
150 trypsinisation (Xu *et al*, 2010). Using this method, we investigated the ubiquitylome of
151 SVEC4-10 cells treated to undergo CICD. Mass spectrometry proteomic analysis
152 revealed a significant change in the ubiquitylome of CICD treated SVEC4-10 cells
153 compared to untreated (**Figure 2A**). Gene-ontology (GO) term analysis and manual
154 curation of proteins using MitoCarta 3.0 (Rath *et al*, 2021) revealed that most peptides
155 (approx. 80%) that gained a ubiquitin modification after MOMP were mitochondrially
156 localised (**Figures 2B – D, Supplemental table 1**). Ubiquitylated mitochondrial
157 proteins were not confined to one mitochondrial compartment, with broadly similar
158 numbers of ubiquitylated proteins characterised as being localised to the mitochondrial
159 outer membrane or mitochondrial inner membrane (**Figure 2B** and **Supplemental**
160 **Table 1**). Notably, some proteins with increased ubiquitylation have been defined as
161 being localised to the mitochondrial matrix, possibly reflecting mitochondrial inner
162 membrane permeabilisation that we and others have reported previously (**Figure 2B**
163 and **Supplemental Table 1**) (McArthur *et al.*, 2018; Riley *et al.*, 2018). These data
164 demonstrate promiscuous ubiquitylation of mitochondrial proteins following MOMP.

165

166

167

Mitochondrial protein ubiquitylation encompasses K63-ubiquitin linkages

Protein ubiquitylation is highly complex with specific ubiquitin linkages conferring distinct biological functions. For instance, K48 ubiquitin linkages are typically associated with targeting proteins for proteasomal degradation, whereas K63 ubiquitylation has signalling functions (Komander & Rape, 2012). Given this, we investigated the type of ubiquitin linkages that MOMP triggers. SVEC4-10 cells were treated to undergo CICD, and the mitochondrial enriched fraction was blotted for K48- and K63-ubiquitin linkages using linkage specific antibodies (**Figure 3A**). This revealed an increase in K63-linked ubiquitin, but not K48-linked ubiquitin, in the mitochondrial fraction specifically during CICD. K63-linked ubiquitylation of mitochondria was also detected upon CICD by immunofluorescence (**Figure 3B** and **3C**). Finally, we made use of GFP-fused ubiquitin binding domains (UBDs) developed to specifically visualise K63 and linear M1 ubiquitin linkages (Hrdinka *et al*, 2016). Consistent with our previous data, extensive K63-linked ubiquitin was detected on mitochondria following CICD (**Figure 3D** and **3E**). In contrast, mitochondrial localisation of M1-specific UBDs was observed in a smaller percentage of cells analysed. These data reveal that upon MOMP, mitochondrial proteins are enriched in K63-ubiquitin linkages.

Mitochondrial ubiquitylation recruits the essential NF-κB adaptor NEMO promoting NF-κB activation

We next sought to understand potential biological functions of mitochondrial ubiquitylation following MOMP. Our previous data demonstrated that NF-κB is activated following MOMP, contributing to anti-tumorigenic effects of CICD (Giampazolias *et al.*, 2017). This finding, coupled to the well-established connection

between K63-ubiquiylation and inflammatory signalling (Madiraju *et al*, 2022), led us to investigate if mitochondrial ubiquitylation may be involved in NF-κB activation during CICD. NEMO, an essential adaptor protein in canonical NF-κB signalling, initiates NF-κB activity through ubiquitin binding. Given this, we examined the localisation of NF-κB essential modulator (NEMO) under conditions of MOMP, by expressing GFP-NEMO in U2OS cells (**Figures 4A** and **4B**). Importantly, robust mitochondrial translocation of GFP-NEMO occurred upon MOMP in a BAX/BAK-dependent manner. To investigate if ubiquitylation was required for mitochondrial recruitment of NEMO we used the E1 inhibitor TAK-243 to block ubiquitylation (Hyer *et al*, 2018). TAK-243 treatment effectively blocked mitochondrial ubiquitylation and mitochondrial recruitment of GFP-NEMO, (**Figure 4C-D** and **Supplemental Figure 2A**). In contrast, blocking the ubiquitin-like modification neddylation, using NAE1 inhibitor MLN4924 (Soucy *et al*, 2009), did not result in reduced ubiquitylation and GFP-NEMO translocation in SVEC4-10 cells (**Supplemental Figure 2B - D**).

M1-ubiqutin linkages are often essential for NEMO activation, through binding the UBAN domain on NEMO (Rahighi *et al*, 2009). Additionally, the C-terminal zinc finger (ZF) domain of NEMO can enhance the binding of K63-ubiquitin chains to the UBAN (Cordier *et al*, 2009; Laplantine *et al*, 2009). To determine which domain(s) are required for ubiquitin-dependent recruitment after MOMP, mutant versions of NEMO disrupting the ability of the UBAN (D311N) or C-terminus (ΔZF) to bind ubiquitin were generated. Both non-ubiquitin binding mutants of NEMO failed to be recruited to the mitochondria after MOMP (**Figure 4E** and **4F**) suggesting that binding to K63-ubiquitin chains is required. To extend these findings, we made use of murine embryonic fibroblasts (MEFs) deficient in HOIP, the catalytic subunit of LUBAC E3 ligase complex

required for M1-linked ubiquitylation (Peltzer *et al*, 2014). Importantly, mitochondrial recruitment of GFP-NEMO was not impaired in HOIP-deficient MEFs (**Supplemental Figures 3A** and **3B**). These data demonstrate that K63-linked ubiquitylation, but not M1-linked ubiquitylation, is required for NEMO recruitment to the mitochondria.

We next determined if mitochondrial recruitment of NEMO facilitates NF-κB activation. SVEC4-10 cells expressing wild-type and non-ubiquitin binding variants of GFP-NEMO (D311N and ΔZF) were treated to engage CICD and NF-κB activation was determined by nuclear NF-κB p65 translocation. In contrast to wild-type NEMO, both non-ubiquitin binding variants of NEMO significantly inhibited NF-κB activation, as determined by a reduction in nuclear p65 (**Figure 4G** and **4H**). Similar experiments were performed in SVEC4-10 cells treated with siRNA to deplete endogenous murine NEMO (**Supplemental Figures 3C - E**). Depletion of NEMO in parental SVEC4-10 cells completely abolished nuclear p65 translocation. As expected, this was rescued by ectopic expression of human GFP-NEMO. In contrast, expression of human GFP-NEMOD311N failed to restore NF-κB p65 nuclear translocation, agreeing with our previous data. These data support a model whereby K63-ubiquitylation of mitochondria following MOMP enables NEMO recruitment leading to NF-κB activation.

Ubiquitin-dependent NF-κB activation after MOMP is independent of canonical mitochondrial E3 ligases

Through MOMP, our findings directly link mitochondrial integrity to mitochondrial ubiquitylation and pro-inflammatory signalling. We next sought to identify which ubiquitin E3 ligase(s) may be responsible for mitochondrial ubiquitylation. One candidate is the E3 ligase Parkin, since active Parkin causes

widespread ubiquitylation of mitochondrial proteins (Sarraf *et al*, 2013). Nonetheless, both SVEC4-10 and U2OS cells used in our studies do not express detectable Parkin (**Figure 5A**), arguing that mitochondrial ubiquitylation following MOMP does not require Parkin. Parkin activity requires the kinase PINK1. Interestingly, PINK1 can also activate alternative E3 ligases such as ARIH1 (Villa *et al*, 2017). To investigate a potential role for PINK1, we generated PINK1^{CRISPR} SVEC4-10 cell lines (**Supplemental Figure 4A**). Confirming functional deletion, cells lacking PINK1 failed to recruit YFP-Parkin to mitochondria following CCCP treatment, in contrast to EMPTY^{CRISPR} cells (**Supplemental Figure 4B**). YFP-Parkin was not recruited to mitochondria after MOMP irrespective of PINK1 deletion (**Supplemental Figure 4B**). Importantly, recruitment of GFP-NEMO was not impaired by the deletion of PINK1 (**Figure 5B** and **5C**) indicating that PINK1 does not have a role in ubiquitin-dependent recruitment of NEMO after MOMP. The mitochondrial resident E3 ligases MUL1 (also called MAPL) and MARCH5 have roles in various cellular processes such as mitochondrial dynamics, protein import, cell death and inflammation (Braschi *et al*, 2009; Haschka *et al*, 2020; Phu *et al*, 2020; Shiiba *et al*, 2020). Single and double knockout MUL1^{CRISPR} and MARCH5^{CRISPR} SVEC4-10 cell lines were generated (**Supplemental Figure 4C** and **4D**), however no differences in IκBα phosphorylation, a marker for NF-κB activation, were observed (**Figure 5D**). Moreover, no impact on mitochondrial ubiquitylation following MOMP was observed in SVEC4-10 MUL1MARCH5^{CRISPR} cells (**Figures 5E-F**). Interestingly, MARCH5 is degraded upon MOMP (**Figure 5D**) indicating that its ubiquitylation observed in the ubiquitin remnant proteomics study might be linked to proteasomal degradation (**Supplemental Table 1**). The E3 ligase XIAP was previously described for its involvement in the recruitment of endolysosomes through ubiquitylation of mitochondrial proteins after MOMP

(Hamacher-Brady *et al*, 2014). XIAP^{CRISPR} SVEC4-10 cell lines were generated to validate the importance of XIAP in mitochondrial-driven inflammation (**Supplemental Figure 4E**). No differences were observed in expression of pro-inflammatory cytokines after MOMP (**Supplemental Figure 4F**), despite observing a small reduction in the percentage of cells with mitochondrial ubiquitylation and GFP-NEMO recruitment (**Figure 5G** and **5H**). Combined, these data demonstrate that established mitochondrial E3 ligases are not required for mitochondrial ubiquitylation following MOMP.

Ubiquitin-dependent mitochondrial inflammation is regulated by mitochondrial outer membrane integrity

As discussed, mitochondrial apoptosis requires BAX and BAK activation leading to MOMP. We next sought to define if pro-inflammatory mitochondrial ubiquitylation was specific to mitochondrial apoptosis or initiated due to loss of mitochondrial integrity. For this purpose, we used the compound raptinal that can cause MOMP independent of BAX and BAK (Heimer *et al*, 2019; Palchaudhuri *et al*, 2015). In agreement, BAX/BAK deficient SVEC4-10 cells were protected against cell death induced by BH3-mimetics but remained sensitive to raptinal-induced cell death in a caspase-dependent manner (**Supplementary Figures 5A** and **B**). We next investigated GFP-NEMO translocation and mitochondrial ubiquitylation following raptinal treatment in BAX/BAK-deleted SVEC4-10 cells. Importantly, raptinal treatment led to robust mitochondrial ubiquitylation and GFP-NEMO translocation independently of BAX and BAK (**Figure 6A** and **6B**). Consistent with this, nuclear translocation of p65 was also observed in BAX/BAK deleted cells following raptinal treatment (**Figure 6C** and **6D**). Finally, increased transcription of NF-κB targets *Kc* and *Tnf* was detected

following raptinal treatment in BAX/BAK-deleted SVEC4-10 cells (**Figure 6E**). Congruent with earlier findings, BH3-mimetic induced ubiquitylation, NEMO translocation and NF-κB activity required BAX and BAK (**Figure 6A-E**). These data demonstrate that loss of mitochondrial outer membrane integrity is sufficient to induce mitochondrial ubiquitylation leading to NEMO recruitment and an NF-κB dependent inflammatory response.

Discussion

We find that upon disruption of mitochondrial outer membrane integrity, mitochondria are promiscuously ubiquitylated; numerous proteins localising to both outer and inner mitochondrial membranes were found to be ubiquitylated. Investigating the functions of mitochondrial ubiquitylation, unexpectedly, we found that degradation of mitochondria could occur independently of canonical autophagy. We found that mitochondrial ubiquitylation directly promotes inflammatory NF-κB activation through mitochondrial recruitment of the adaptor molecule NEMO. These data connect mitochondrial outer membrane integrity to direct activation of NF-κB activity, contributing to the pro-inflammatory effects of MOMP.

Given the bacterial ancestry of mitochondria, our findings raise striking parallels with cell intrinsic responses to bacterial infection. For instance, ubiquitylation of intracellular *Salmonella* Typhimurium serves as a platform to initiate pro-inflammatory NF-κB signalling as an innate immune response (Noad *et al*, 2017; van Wijk *et al*, 2017)}. Notably, the mitochondrial inner membrane and bacterial membranes share similarities, for instance enrichment in cardiolipin (Vringer & Tait, 2022). We speculate that upon cytosolic exposure, the mitochondrial inner membrane may represent a damage-associated molecular pattern (DAMP) eliciting ubiquitylation, NEMO recruitment and inflammation. Nonetheless, distinct differences exist between NEMO recruitment leading to NF-κB activation on invading bacteria and permeabilised mitochondria. The most striking distinction is that, unlike bacteria, M1-linked ubiquitylation is not required for recruitment of NEMO to permeabilised mitochondria. This is best evidenced by mitochondrial recruitment of NEMO in cells deficient in HOIP, the catalytic subunit of LUBAC complex required for M1-linked ubiquitylation.

Instead, NEMO recruitment to mitochondria appears dependent on its ability to bind K63-ubiquitylated proteins, indeed we observe extensive K63-linked (but not degradative K48-linked) mitochondrial ubiquitylation upon MOMP. Interestingly, a recent study has shown that mitochondria amplify TNF induced NF-κB signalling (Wu *et al*, 2022). In this paradigm, the mitochondrial outer membrane serves as a platform for LUBAC activity enhancing linear M1-linked ubiquitylation of NEMO. Together with our data, this positions mitochondria in different contexts as both initiators and amplifiers of NF-κB dependent signalling.

Mechanistic questions remain – not least the identity of the ubiquitin E3 ligase(s) required for MOMP induced ubiquitylation. Our data argues against key roles for PINK1/Parkin, XIAP or resident mitochondrial ubiquitin ligases such as MARCH5 and MUL1. Secondly, what properties of permeabilised mitochondria that initiates ubiquitylation remains unknown. Importantly, our data shows that mitochondrial ubiquitylation occurs upon loss of mitochondrial outer membrane integrity, independent of how this is achieved. This is best evidenced by MOMP engaged by either BAX/BAK or using the drug raptinal (in BAX/BAK null cells) both cause mitochondrial ubiquitylation, NEMO recruitment and NF-κB activation. While speculative, possibly proteins located on the inner mitochondrial membrane when exposed to the cytosol recruit and activate cytosolic ubiquitin ligases.

Our initial premise for this study stemmed from the hypothesis that mitochondrial ubiquitylation may serve as targeting signal for mitophagy, akin to PINK1/Parkin mediated mitophagy. Surprisingly, we found that mitochondrial degradation occurred in cells deficient in canonical autophagy. While this doesn't

349 negate a role for autophagy in promoting removal of permeabilised mitochondria, it
350 demonstrates that autophagy not essential. Along these lines, we and others have
351 previously found that upon MOMP, the mitochondrial outer membrane can be
352 completely lost leaving what we called mito-corpses (Ader *et al*, 2019; Riley *et al.*,
353 2018). Whether autophagy independent degradation of permeabilised mitochondria
354 occurs in a regulated manner remains an open question.
355
356 In summary, our data reveals a novel direct connection between mitochondrial
357 function and engagement of inflammation, where disruption of mitochondrial integrity
358 initiates pro-inflammatory NF-κB signalling through extensive ubiquitylation and
359 NEMO recruitment. Given the numerous emerging functions of MOMP induced
360 inflammation, ranging from senescence to innate and anti-tumour immunity, basic
361 understanding of this process may reveal new therapeutic opportunities.
362
363

Materials and Methods

Cell culture and chemicals

HEK293FT, SVEC4-10, MEFs and U2OS cells were cultured in high glucose DMEM supplemented with 10% FBS (Gibco #10438026), 2 mM glutamine (Gibco #25030081) and 1 mM sodium pyruvate (Gibco #11360070). Cells were cultured in 21% O_2 and 5% CO_2 at 37 ºC. MEF *Tnf*$^{-/-}$ *Hoip*$^{+/+}$ and MEF *Tnf*$^{-/-}$ *Hoip*$^{-/-}$ cell lines have been described before (Peltzer ***et al.***, 2014). SVEC4-10 cells were purchased from ATCC. All cell lines were routinely tested for mycoplasma.

The following chemicals were used in this study: ABT-737 (APEXBIO #A8193), S63845 (Chemgood #C-1370), Q-VD-OPh (AdooQ Bioscience #A14915-25), Doxycycline hyclate (Sigma-Aldrich #D9891), TAK-243 (MedChemExpress #HY-100487), MLN4924 (Selleck Chemical #S7109), MG-132 (Selleck Chemical #S2619), and raptinal (Millipore Sigma #SML1745).

Viral transfection

Overexpression and CRISPR cells lines were generated using lenti- or retroviral infection. For lentiviral transfections 1 µg VSVG (Addgene #8454) and 1.86 µg psPAX2 (Addgene #12260) were used. For retroviral transfections 1 µg VSVG and 1.86 µg HIV gag-pol (Addgene #14887) were used. For both transfections 5 µg of plasmid was used. HEK293FTs were transfected using lipofectamine 2000 or lipofectamine 3000 according to manufacturer's instructions. After two days, virus-containing media was removed from the HEK293FTs and supplemented with 10 µg/ml polybrene before transferring to target cells. Two days after infection cells were selected using 2 µg/mL puromycin, 10 µg/mL blasticidin or 800 µg/mL neomycin.

Some U2OS and SVEC4-10 lines expressing GFP were sorted for GFP expression instead of antibiotic selection.

The M6PblastGFP-NEMO, PMD-OGP and PMD-VSVG plasmids were gifted by Felix Randow. The pLenti-CMV-TetRepressor, pDestination-eGFP-NES, pDestination-eGFP-SK63-NES and pDestination-eGFP-NCM1-NES plasmids were gifted by Mads Gyrd-Hansen. CRISPR cell lines were generated using lentiCRISPRv1 or lentiCRISPRv2 vector (Addgene #52961) containing puromycin, blasticidin and neomycin resistance.

Human *BAK* 5'- GCCATGCTGGTAGACGTGTA -3'

Human *BAX* 5'- AGTAGAAAAGGGCGACAACC -3'

Human *ATG5* 5'- AAGAGTAAGTTATTTGACGT -3'

Human *ATG7* 5'- GAAGCTGAACGAGTATCGGC -3'

Mouse *Bak* 5'- GCGCTACGACACAGAGTTCC -3'

Mouse *Bax* 5'- CAACTTCAACTGGGGCCGCG -3'

Mouse *March5* 5'- AAGTACTCGGCGTTGCACTG -3'

Mouse *Mul1* 5'- TATATGGAGTACAGTACGG -3'

Mouse *Pink1* 5'- CTGATCGAGGAGAAGCAGG -3'

Mouse *Xiap* 5'- CATCAACATTGGCGCGAGCT -3'

Generation of GFP-NEMOD311N and GFP-NEMOΔZF

GFP-NEMOD311N and GFP-NEMOΔZF were cloned into a pBABE-puro vector using EcoRI and BamHI restriction sites. GFP-NEMOD311N was cloned into the pBABE vector using Gibson assembly. NEMOD311N was obtained by PCR of pGEX-NEMOD311N (Addgene #11968). GFP was obtained by PCR of a GFP-containing

plasmid. GFP-NEMOΔZF was obtained by PCR of the M6P-GFP-NEMO plasmid (gifted by Felix Randow), thereby removing the last 25 amino acids of wildtype NEMO.

GFP 5'- tctaggcgccggccggatccATGGTGAGCAAGGGCGAG -3'

GFP 3'- cagaaccaccaccaccCTTGTACAGCTCGTCCATGC -5'

NEMOD311N

5'-ctgtacaagggtggtggtggttctggtggtggtggttctAATAGGCACCTCTGGAAG -3'

NEMOD311N 3'- accactgtgctggcgaattcCTACTCAATGCACTCCATG -5'

GFP-NEMOΔZF 5'- TAAGCA GGATTCATGGTGAGCAAGGGCGAGGAG -3'

GFP-NEMOΔZF 3'- TGCTTA GAATTC CTAGTCAGGTGGCTCCTCGGGGG -5'

ICE analysis for CRISPR

Genomic DNA was isolated from the empty vector and CRISPR cells. A PCR reaction for the CRISPR'ed region was set-up using Phusion DNA polymerase according to manufacturer's instructions. The reactions were run on 2% agarose gel and bands of correct size were isolated and purified using the GeneJET Gel Extraction kit. Samples were sequenced by Eurofins genomics and analysed using ICE software by Synthego.

Mouse *March5* 5'- TCCTGGCCTGAAGGGTAGGGGA -3'

Mouse *March5* 3'- CCTCTTCCTTCCCCCACCCCAA -5'

Mouse *Mul1* 5'- GGGTCGCAGGTGATTTCGAGGC -3'

Mouse *Mul1* 3'- CACGTTGGAATCACCCCTGCCT -5'

Mouse *Pink1* 5'- TGTTGTTGTCCCAGACGTTTGT -3'

Mouse *Pink1* 3'- TAAATTGCCCAATCACGGCTCA -5'

Knockdown using siRNA

SVEC4-10 cells were transfected with 20 nM siGENOME *Nemo* SMARTpool (Horizon Discovery #M-040796-01-0005) or siGENOME non-targeting control (Dharmacon #D0012061305) using lipofectamine RNAiMAX (Invitrogen #1377075). Experiments were performed 48 hours after transfection.

RT-qPCR

RNA was isolated using the GeneJET RNA isolation kit (Thermo Fisher Scientific #K0732) according to manufacturer's instructions. Genomic DNA was digested using an on-column DNase step (Sigma-Aldrich #04716728001) for 15 minutes. RNA was converted into cDNA using the High Capacity cDNA Reverse Transcriptase kit (Thermo Fisher Scientific #43-688-13) according to manufacturer's instructions. cDNA was synthesised according to the following steps: 25 °C for 10 minutes, 37 °C for 120 minutes and 85 °C for 5 minutes.

RT-qPCR was performed by using the Brilliant III SYBR® Green QPCR Master Mix (Agilent #600882) or DyNAmo HS SYBR Green (Thermo Scientific #F410L) and the QuantStudio 3. The following RT-qPCR cycling parameters were used: initial denaturation on 95 °C for 10 minutes, 40 cycles of 95 °C for 20 seconds, 57 °C for 30 seconds and 72 °C for 30 seconds, finished by a dissociation step 65-95 °C (0.5 °C/second). Samples were run in technical triplicates. Fold change expression was determined using the $2^{-\Delta\Delta CT}$ method.

<u>cDNA</u>

Mouse *Actin* 5'- CTAAGGCCAACCGTGAAAAG -3'

Mouse *Actin* 3'- ACCAGAGGCATACAGGGACA -5'

Mouse *Tnf-α* 5'- GTCCCCAAAGGGATGAGAAG -3'

Mouse *Tnf-α* 3'- CACTTGGTGGTTTGCTACGAC -5'

Mouse *Kc* 5'- GGCTGGGATTCACCTCAAGAA -3'

Mouse *Kc* 3'- GAGTGTGGCTATGACTTCGGTT -5'

Mouse *Ccl5* 5'- CTGCTGCTTTGCCTACCTCT -3'

Mouse *Ccl5* 3'- CGAGTGACAAACACGACTGC -5'

DNA

Human *CYTB* 5'- GCCTGCCTGATCCTCCAAAT -3'

Human *CYTB* 3'- AAGGTAGCGGATGATTCAGCC -5'

Human *GAPDH* 5'- TGGGGACTGGCTTTCCCATAA -3'

Human *GAPDH* 5'- CACATCACCCCTCTACCTCC -3'

Western blotting

Cells were lysed in RIPA buffer (10 mM Tris-HCl (pH 7.4), 150 mM NaCl, 1.2 mM EDTA, 1% Triton X-100 and 0.1% SDS supplemented with cOmplete protease inhibitors) and proteins were isolated by maximal centrifugation (15,000 rpm) for 10 minutes. Lysates were loaded on 8, 10 or 12% gels and transferred onto nitrocellulose membranes. The membranes were blocked with 5% milk or BSA in TBS for 1 hour followed by overnight incubation of 1:1000 dilution of primary antibodies in 5% milk or BSA in TBST. The next day membranes were incubated with a 1:10,000 dilution of secondary antibodies for 1 hour and imaged on the Li-cor CLx. Primary antibodies used are actin (Sigma #A4700), ATG5 (CST #8540), ATG7 (CST #8558), LC3 (CST #2775), BAK (CST #12105), BAX (CST #2772), NEMO (Abcam #178872), FK2 (ENZO #BML-PW8810-0100), HSP60 (Santa Cruz #sc-13115), p-IκBα (CST #2859),

IκBα (CST #4814), K48-ubiquitin (CST #8081), K63-ubiquitin (Merck #05-1308), NEDD8 (Abcam #AB81264), Parkin (Santa Cruz #sc-32282), SMAC (Abcam #AB32023), TOMM20 (Proteintech #11082-1-AP), UBCJ2 (ENZO #ENZ-ABS840-0100), Membrane Integrity Antibody cocktail (Abcam #ab110414), COXIV (CST #11967), MARCH5 (EMD Millipore #06-1036) and XIAP (BD #610716). Secondary antibodies used are goat anti-rabbit IgG (H+L) Alexa Fluor Plus 800 (Invitrogen #A32735), goat anti-mouse IgG (H+L) Alexa Fluor 680 (Invitrogen #A21057) and goat anti-mouse IgG (H+L) Dylight 800 (Invitrogen #SA535521).

Mitochondrial isolation using digitonin

Cells were lysed in digitonin lysis buffer (0.25 M sucrose, 700 mM Tris-HCl pH 8 and 100 µg/mL digitonin) for 10 minutes on ice. The mitochondrial fraction was pelleted at 3000*g* for 5 minutes. Supernatant was stored as the non-mitochondrial fraction, the pellet was resuspended in RIPA lysis buffer and stored on ice for 20 minutes followed by centrifugation for 10 minutes at maximum speed (15,000 rpm). Supernatant was taken as mitochondrial fraction.

Mitochondrial isolation using douce homogeniser

Cells were resuspended in mitochondrial isolation buffer (200 mM mannitol, 70 mM sucrose, 10 mM HEPES, 1 mM EGTA, pH 7.0, cOmplete protease inhibitor). After resuspension cells were homogenised using the dounce tissue grinder by performing 50 strokes up/down manually and centrifuged at 2000 rpm for 5 minutes. Supernatant was collected and pellet was resuspended in mitochondrial isolation buffer and spun down as previously described. Supernatant from both spins were combined and spun down at 9000 rpm for 5 minutes. The supernatant was kept as non-mitochondrial

fraction. The pellet was resuspended in RIPA buffer and placed on ice for 20 minutes followed by centrifugation at maximum speed (15,000 rpm) for 10 minutes. Supernatant was kept as mitochondrial fraction.

Immunofluorescent staining

Cells were fixed using 4% PFA for 15 minutes, followed by a 15 minutes permeabilization step using 0.2% Triton X-100. Samples were blocked using 2% BSA in PBS for 1 hour and incubated with primary antibody in 2% BSA overnight. The following day samples were incubated with secondary antibody in 2% BSA. Primary antibodies used are COXIV (CST #11967 and #4850), cytochrome *c* (BD #556432), FK2 (ENZO #BML-PW8810-0100), HSP60 (Santa Cruz #sc-13115), K63-ubiquitin (Merck #05-1308), p65 (CST #8242), TOMM20 (CST #42406 and Proteintech #11082-1-AP) and UBCJ2 (ENZO #ENZ-ABS840-0100). Secondary antibodies used are Alexa Fluor 488 goat anti-rabbit IgG (H+L) (Invitrogen #A11034), Alexa Fluor 488 goat anti-mouse IgG (H+L) (Invitrogen #A11029), Alexa Fluor 568 goat anti-rabbit IgG (H+L) (Invitrogen #A11011), Alexa Fluor 568 goat anti-mouse IgG (H+L) (Invitrogen #A11004), Alexa Fluor 647 goat anti-rabbit IgG (H+L) (Invitrogen #A21245) and Alexa Fluor 647 goat anti-mouse IgG (H+L) (Invitrogen #A21236). Coverslips were mounted using Vectashield with or without DAPI.

Confocal microscopy

Cells were imaged using the Nikon A1R confocal microscope using all four lasers (405 nm, 488 nm, 561 nm and 638 nm) and images are acquired using sequential scanning. For p65 staining the 40x NA 1.30 oil-immersion objective was used, while the 60x 1.40 NA oil-immersion objective was used to determine ubiquitin, GFP-NEMO and YFP-

Parkin puncta. Images were analysed using ImageJ version 2.1.0/1.53c and cells were counted using the cell counter plugin. Images may be displayed using pseudocolours.

Cell death assays using Incucyte

Cell death assays were performed using Incucyte ZOOM from Sartorius. Cell death was measured by Sytox Green inclusion (Thermo Fisher Scientific #S7020). Images were taken every hour with a 10x objective. Starting confluency was used to normalisation.

Isolation of peptides containing ubiquitin remnants

Peptides containing ubiquitin remnant motifs were isolated using the PTMScan® Ubiquitin Remnant Motif (K--GG) Kit (CST #5562) according to manufacturers' instructions. Isolation of ubiquitin remnants was performed on 4 independent repeats for both conditions (4.4 mg protein per sample). Cellular localisation of proteins was determined using Uniprot and Proteinatlas. Mitochondrial localisation was determined using MitoCarta 3.0. GO enrichment analysis was performed using PANTHER classification system.

Mass spectrometry

Peptides were separated by nanoscale C18 reverse-phase liquid chromatography using an EASY-nLC II 1200 (Thermo Scientific) coupled to an Orbitrap Fusion Lumos mass spectrometer (Thermo Scientific). Elution was performed at a flow rate of 300 nL/min using a binary gradient, into a 50 cm fused silica emitter (New Objective) packed in-house with ReproSil-Pur C18-AQ, 1.9 µm resin (Dr Maisch GmbH), for a total duration of 135 minutes. Packed emitter was kept at 50 °C by column oven

(Sonation) integration into the nanoelectrospray ion source (Thermo Scientific). Eluting peptides were electrosprayed into the mass spectrometer using a nanoelectrospray ion source. To decrease air contaminants signal level an Active Background Ion Reduction Device (EDI Source Solutions) was used. Data acquisition was performed using Xcalibur software (Thermo Scientific). A full scan over mass range of 350-1400 m/z was acquired at 120,000 resolution at 200 m/z. Higher energy collision dissociation fragmentation was performed on the 15 most intense ions, and peptide fragments generated were analysed in the Orbitrap at 15,000 resolution.

The MS Raw data were processed using MaxQuant software version 1.6.3.3 and searched with Andromeda search engine (Cox *et al*, 2011) querying SwissProt (Consortium 2019) Mus musculus (20/06/2016; 57,258 entries). First and main searched were performed with precursor mass tolerances of 20 ppm and 4.5 ppm, respectively, and MS/MS tolerance of 20 ppm. The minimum peptide length was set to six amino acids and specificity for trypsin cleavage was required. Methionine oxidation, N-terminal acetylation and di-Gly-lysine were specified as variable modifications, whereas cysteine carbamidomethylation was set as fixed modification. The peptide, protein, and site false discovery rate (FDR) was set to 1%. All MaxQuant outputs were analysed with Perseus software version 1.6.2.3 (Tyanova *et al*, 2016). The MaxQuant output GlyGly (K)sites.txt file was use for quantification of Ubiquitylated peptides. From the GlyGly (K)Sites.txt file, Reverse and Potential Contaminant flagged peptides (defined as MaxQuant output) were removed. To determine significanly changing ubiquitylated peptides a Student t-test with a 1% FDR (permutation-based) was applied using the peptide intensities included in the GlyGly (K)Sites table. Missing values were imputated separately for each column (width 0.3, down shift 1.4). Only

ubiquitylated peptides having: “score diff” greater than 5, a localisation probability higher than 0.75, and are robustly quantified in three out of four replicate experiments were included in the analysis.

Data availability

The raw files and the MaxQuant search results files have been deposited to the ProteomeXchange Consortium (Deutsch *et al*, 2020) via the PRIDE partner repository (Perez-Riverol *et al*, 2022) with the dataset identifier PXD040192. Data are available via ProteomeXchange with identifier PXD040192.

For reviewer access: **Username:** reviewer_pxd040192@ebi.ac.uk **Password:** YDEFnxY5

Statistics

Statistics was performed using Prism 9. All data represent mean ± standard error of the mean (SEM) unless indicated differently.

* $p < 0.05$, ** $p < 0.01$, *** $p < 0.001$, **** $p < 0.0001$

Acknowledgements

This research was supported by funding from the Cancer Research UK (A20145; S.W.G.T.)(A29256; D.T.H.). Stand Up to Cancer campaign for CRUK A29800 to S.Z.; A31287 to CRUK Beatson Institute, A18076 to CRUK Glasgow Centre, A17196 to CRUK Beatson Institute Advanced Technology Facilities. H.W. is supported by an Alexander von Humboldt Foundation Professorship Award, a Cancer Research UK Programme Grant (A27323), a Wellcome Trust Investigator Award (214342/Z/18/Z), a Medical Research Council Grant (MR/S00811X/1) and three collaborative research

613 centre grants funded by Deutsche Forschungsgemeinschaft (DFG, German Research
614 Foundation): SFB1399, Project C06; SFB1530-455784452, Project A03; and
615 SFB1403–414786233. M.G-H. is supported by the LEO foundation and The Novo Nordisk
616 Foundation (NNF20OC0059392). We thank Rosalie Heilig, Asma Ahmed and Catherine
617 Winchester for critical reading of the manuscript. The authors declare that they have
618 no conflict of interest

References

Ader NR, Hoffmann PC, Ganeva I, Borgeaud AC, Wang C, Youle RJ, Kukulski W (2019) Molecular and topological reorganizations in mitochondrial architecture interplay during Bax-mediated steps of apoptosis. *Elife* 8

Bock FJ, Tait SWG (2020) Mitochondria as multifaceted regulators of cell death. *Nat Rev Mol Cell Biol* 21: 85-100

Braschi E, Zunino R, McBride HM (2009) MAPL is a new mitochondrial SUMO E3 ligase that regulates mitochondrial fission. *EMBO Rep* 10: 748-754

Brokatzky D, Dorflinger B, Haimovici A, Weber A, Kirschnek S, Vier J, Metz A, Henschel J, Steinfeldt T, Gentle IE *et al* (2019) A non-death function of the mitochondrial apoptosis apparatus in immunity. *EMBO J* 38

Cao K, Riley JS, Heilig R, Montes-Gomez AE, Vringer E, Berthenet K, Cloix C, Elmasry Y, Spiller DG, Ichim G *et al* (2022) Mitochondrial dynamics regulate genome stability via control of caspase-dependent DNA damage. *Dev Cell* 57: 1211-1225 e1216

Chapman JS HS, Stella Victorelli , Helene Martini , Joel Riley , Catherine Cloix , Gerald Shadel , Jair Machado Espindola Netto , Diana Jurk , Anthony Lagnado , Lilian Sales Gomez , Joshua Farr , Dominik Saul , Rebecca Reed , Laura Greaves , Derek Mann , Claudio Akio Masuda , Sundeep Khosla , Haiming Dai , Nathan LeBrasseur , Viktor Korolchuk , Xue Shae , Peter Adams , Stephen Tait , Maria Grazia Vizioli , Alva

Sainz Castillo , Scott Kaufmann , Zhixun Dou , George Kelly , Ella Hall-Younger , Karolina Szczepanowska , Nicholas Pirius Sub-lethal apoptotic stress enables mtDNA release during senescence and drives the SASP. *Research Square* https://doi.org/10.21203/rs.3.rs-1247316/v1

Colell A, Ricci JE, Tait S, Milasta S, Maurer U, Bouchier-Hayes L, Fitzgerald P, Guio-Carrion A, Waterhouse NJ, Li CW *et al* (2007) GAPDH and autophagy preserve survival after apoptotic cytochrome c release in the absence of caspase activation. *Cell* 129: 983-997

Cordier F, Grubisha O, Traincard F, Veron M, Delepierre M, Agou F (2009) The zinc finger of NEMO is a functional ubiquitin-binding domain. *J Biol Chem* 284: 2902-2907

Cox J, Neuhauser N, Michalski A, Scheltema RA, Olsen JV, Mann M (2011) Andromeda: a peptide search engine integrated into the MaxQuant environment. *J Proteome Res* 10: 1794-1805

Deutsch EW, Bandeira N, Sharma V, Perez-Riverol Y, Carver JJ, Kundu DJ, Garcia-Seisdedos D, Jarnuczak AF, Hewapathirana S, Pullman BS *et al* (2020) The ProteomeXchange consortium in 2020: enabling 'big data' approaches in proteomics. *Nucleic Acids Res* 48: D1145-D1152

Giampazolias E, Zunino B, Dhayade S, Bock F, Cloix C, Cao K, Roca A, Lopez J, Ichim G, Proics E *et al* (2017) Mitochondrial permeabilization engages NF-kappaB-dependent anti-tumour activity under caspase deficiency. *Nat Cell Biol* 19: 1116-1129

660 Hamacher-Brady A, Choe SC, Krijnse-Locker J, Brady NR (2014) Intramitochondrial
661 recruitment of endolysosomes mediates Smac degradation and constitutes a novel
662 intrinsic apoptosis antagonizing function of XIAP E3 ligase. *Cell Death Differ* 21: 1862-
663 1876

664 Han C, Liu Z, Zhang Y, Shen A, Dong C, Zhang A, Moore C, Ren Z, Lu C, Cao X *et al*
665 (2020) Tumor cells suppress radiation-induced immunity by hijacking caspase 9
666 signaling. *Nat Immunol* 21: 546-554

667 Haschka MD, Karbon G, Soratroi C, O'Neill KL, Luo X, Villunger A (2020) MARCH5-
668 dependent degradation of MCL1/NOXA complexes defines susceptibility to antimitotic
669 drug treatment. *Cell Death Differ* 27: 2297-2312

670 Heimer S, Knoll G, Schulze-Osthoff K, Ehrenschwender M (2019) Raptinal bypasses
671 BAX, BAK, and BOK for mitochondrial outer membrane permeabilization and intrinsic
672 apoptosis. *Cell Death Dis* 10: 556

673 Hrdinka M, Fiil BK, Zucca M, Leske D, Bagola K, Yabal M, Elliott PR, Damgaard RB,
674 Komander D, Jost PJ *et al* (2016) CYLD Limits Lys63- and Met1-Linked Ubiquitin at
675 Receptor Complexes to Regulate Innate Immune Signaling. *Cell Rep* 14: 2846-2858

676 Hyer ML, Milhollen MA, Ciavarri J, Fleming P, Traore T, Sappal D, Huck J, Shi J, Gavin
677 J, Brownell J *et al* (2018) A small-molecule inhibitor of the ubiquitin activating enzyme
678 for cancer treatment. *Nat Med* 24: 186-193

679 Ichim G, Lopez J, Ahmed SU, Muthalagu N, Giampazolias E, Delgado ME, Haller M,
680 Riley JS, Mason SM, Athineos D *et al* (2015) Limited mitochondrial permeabilization
681 causes DNA damage and genomic instability in the absence of cell death. *Mol Cell* 57:
682 860-872

683 Komander D, Rape M (2012) The ubiquitin code. *Annu Rev Biochem* 81: 203-229

684 Komatsu M, Waguri S, Ueno T, Iwata J, Murata S, Tanida I, Ezaki J, Mizushima N,
685 Ohsumi Y, Uchiyama Y *et al* (2005) Impairment of starvation-induced and constitutive
686 autophagy in Atg7-deficient mice. *J Cell Biol* 169: 425-434

687 Kuma A, Hatano M, Matsui M, Yamamoto A, Nakaya H, Yoshimori T, Ohsumi Y,
688 Tokuhisa T, Mizushima N (2004) The role of autophagy during the early neonatal
689 starvation period. *Nature* 432: 1032-1036

690 Laplantine E, Fontan E, Chiaravalli J, Lopez T, Lakisic G, Veron M, Agou F, Israel A
691 (2009) NEMO specifically recognizes K63-linked poly-ubiquitin chains through a new
692 bipartite ubiquitin-binding domain. *EMBO J* 28: 2885-2895

693 Lartigue L, Kushnareva Y, Seong Y, Lin H, Faustin B, Newmeyer DD (2009) Caspase-
694 independent mitochondrial cell death results from loss of respiration, not cytotoxic
695 protein release. *Mol Biol Cell* 20: 4871-4884

696 Lindqvist LM, Frank D, McArthur K, Dite TA, Lazarou M, Oakhill JS, Kile BT, Vaux DL
697 (2018) Autophagy induced during apoptosis degrades mitochondria and inhibits type
698 I interferon secretion. *Cell Death Differ* 25: 784-796

699 Madiraju C, Novack JP, Reed JC, Matsuzawa SI (2022) K63 ubiquitination in immune
700 signaling. *Trends Immunol* 43: 148-162

701 Marchi S, Guilbaud E, Tait SWG, Yamazaki T, Galluzzi L (2022) Mitochondrial control
702 of inflammation. *Nat Rev Immunol*: 1-15

703 McArthur K, Whitehead LW, Heddleston JM, Li L, Padman BS, Oorschot V,
704 Geoghegan ND, Chappaz S, Davidson S, San Chin H *et al* (2018) BAK/BAX
705 macropores facilitate mitochondrial herniation and mtDNA efflux during apoptosis.
706 *Science* 359

707 McIlwain DR, Berger T, Mak TW (2013) Caspase functions in cell death and disease.
708 *Cold Spring Harb Perspect Biol* 5: a008656

709 Ning X, Wang Y, Jing M, Sha M, Lv M, Gao P, Zhang R, Huang X, Feng JM, Jiang Z
710 (2019) Apoptotic Caspases Suppress Type I Interferon Production via the Cleavage
711 of cGAS, MAVS, and IRF3. *Mol Cell* 74: 19-31 e17

712 Noad J, von der Malsburg A, Pathe C, Michel MA, Komander D, Randow F (2017)
713 LUBAC-synthesized linear ubiquitin chains restrict cytosol-invading bacteria by
714 activating autophagy and NF-kappaB. *Nat Microbiol* 2: 17063

715 Palchaudhuri R, Lambrecht MJ, Botham RC, Partlow KC, van Ham TJ, Putt KS,
716 Nguyen LT, Kim SH, Peterson RT, Fan TM *et al* (2015) A Small Molecule that Induces
717 Intrinsic Pathway Apoptosis with Unparalleled Speed. *Cell Rep* 13: 2027-2036

718 Peltzer N, Rieser E, Taraborrelli L, Draber P, Darding M, Pernaute B, Shimizu Y, Sarr
719 A, Draberova H, Montinaro A *et al* (2014) HOIP deficiency causes embryonic lethality
720 by aberrant TNFR1-mediated endothelial cell death. *Cell Rep* 9: 153-165

721 Perez-Riverol Y, Bai J, Bandla C, Garcia-Seisdedos D, Hewapathirana S,
722 Kamatchinathan S, Kundu DJ, Prakash A, Frericks-Zipper A, Eisenacher M *et al*
723 (2022) The PRIDE database resources in 2022: a hub for mass spectrometry-based
724 proteomics evidences. *Nucleic Acids Res* 50: D543-D552

725 Phu L, Rose CM, Tea JS, Wall CE, Verschueren E, Cheung TK, Kirkpatrick DS, Bingol
726 B (2020) Dynamic Regulation of Mitochondrial Import by the Ubiquitin System. *Mol*
727 *Cell* 77: 1107-1123 e1110

728 Rahighi S, Ikeda F, Kawasaki M, Akutsu M, Suzuki N, Kato R, Kensche T, Uejima T,
729 Bloor S, Komander D *et al* (2009) Specific recognition of linear ubiquitin chains by
730 NEMO is important for NF-kappaB activation. *Cell* 136: 1098-1109

731 Rath S, Sharma R, Gupta R, Ast T, Chan C, Durham TJ, Goodman RP, Grabarek Z,
732 Haas ME, Hung WHW *et al* (2021) MitoCarta3.0: an updated mitochondrial proteome
733 now with sub-organelle localization and pathway annotations. *Nucleic Acids Res* 49:
734 D1541-D1547

735 Ravichandran KS (2011) Beginnings of a good apoptotic meal: the find-me and eat-
736 me signaling pathways. *Immunity* 35: 445-455

737 Riley JS, Quarato G, Cloix C, Lopez J, O'Prey J, Pearson M, Chapman J, Sesaki H,
738 Carlin LM, Passos JF *et al* (2018) Mitochondrial inner membrane permeabilisation
739 enables mtDNA release during apoptosis. *EMBO J* 37

740 Sarraf SA, Raman M, Guarani-Pereira V, Sowa ME, Huttlin EL, Gygi SP, Harper JW
741 (2013) Landscape of the PARKIN-dependent ubiquitylome in response to
742 mitochondrial depolarization. *Nature* 496: 372-376

743 Shiiba I, Takeda K, Nagashima S, Yanagi S (2020) Overview of Mitochondrial E3
744 Ubiquitin Ligase MITOL/MARCH5 from Molecular Mechanisms to Diseases. *Int J Mol*
745 *Sci* 21

746 Soucy TA, Smith PG, Milhollen MA, Berger AJ, Gavin JM, Adhikari S, Brownell JE,
747 Burke KE, Cardin DP, Critchley S *et al* (2009) An inhibitor of NEDD8-activating
748 enzyme as a new approach to treat cancer. *Nature* 458: 732-736

749 Tyanova S, Temu T, Sinitcyn P, Carlson A, Hein MY, Geiger T, Mann M, Cox J (2016)
750 The Perseus computational platform for comprehensive analysis of (prote)omics data.
751 *Nat Methods* 13: 731-740

752 van Wijk SJL, Fricke F, Herhaus L, Gupta J, Hotte K, Pampaloni F, Grumati P, Kaulich
753 M, Sou YS, Komatsu M *et al* (2017) Linear ubiquitination of cytosolic Salmonella
754 Typhimurium activates NF-kappaB and restricts bacterial proliferation. *Nat Microbiol*
755 2: 17066

Vargas JNS, Hamasaki M, Kawabata T, Youle RJ, Yoshimori T (2022) The mechanisms and roles of selective autophagy in mammals. *Nat Rev Mol Cell Biol*

Villa E, Proics E, Rubio-Patino C, Obba S, Zunino B, Bossowski JP, Rozier RM, Chiche J, Mondragon L, Riley JS *et al* (2017) Parkin-Independent Mitophagy Controls Chemotherapeutic Response in Cancer Cells. *Cell Rep* 20: 2846-2859

Vringer E, Tait SWG (2022) Mitochondria and cell death-associated inflammation. *Cell Death Differ*

Wu Z, Berlemann LA, Bader V, Sehr DA, Dawin E, Covallero A, Meschede J, Angersbach L, Showkat C, Michaelis JB *et al* (2022) LUBAC assembles a ubiquitin signaling platform at mitochondria for signal amplification and transport of NF-kappaB to the nucleus. *EMBO J* 41: e112006

Xu G, Paige JS, Jaffrey SR (2010) Global analysis of lysine ubiquitination by ubiquitin remnant immunoaffinity profiling. *Nat Biotechnol* 28: 868-873

Figure 1 Mitochondrial depletion after MOMP does not require autophagy

A) U2OS EMPTY^{CRISPR} and BAX/BAK^{CRISPR} cells treated with 10 μM ABT-737, 2 μM S63845 and 20 μM Q-VD-OPh for 8 or 24 hours. Mitochondrial depletion was assessed by blotting for several mitochondrial proteins. Blot is representative of 3 independent experiments. B) U2OS EMPTY^{CRISPR} and BAX/BAK^{CRISPR} cells were treated with 10 μM ABT-737, 2 μM S62845 and 20 μM Q-VD-OPh for 24 hours. Graphs shows presence of mtDNA relative to gDNA in 3 independent experiments. C) SVEC4-10 cells treated for 1 hour with 10 μM ABT-737, 10 μM S63845 and 30 μM Q-VD-OPh. Mitochondria were isolated using dounce homogeniser. Lysates for blotted for ubiquitin (UBCJ2), SMAC, TOM20, HSP60 and actin. Blots are representative of 2 independent experiments. D) U2OS EMPTY^{CRISPR} and BAX/BAK^{CRISPR} cells treated for 3 hours with 10 μM ABT-737, 2 μM S63845 and 20 μM Q-VD-OPh. Cells were stained for ubiquitin (FK2) and mitochondrial COXIV. Images are representative of 3 independent experiments. Images are maximum projections of Z-stacks with a scale of 20 μm. E) Quantification of panel C showing the percentage of cells with mitochondrial localised ubiquitin puncti. F) U2OS EMPTY^{CRISPR}, ATG5^{CRISPR} and ATG7^{CRISPR} expressing YFP-Parkin were treated with 10 μM ABT-737, 2 μM S63845 and 20 μM Q-VD-OPh for 24 hours. Mitochondrial depletion was assessed by blotting for several mitochondrial proteins. Blot is representative of 3 independent experiments. Statistics for all experiments were performed using two-way ANOVA with Tukey correction. * $p < 0.05$, ** $p < 0.01$, **** $p < 0.0001$.

Figure 2 Widespread ubiquitylation of mitochondrial proteins after MOMP

A) Volcano plot of ubiquitylated proteins in SVEC4-10 cells treated for 3 hours with 10 μM ABT-737, 10 μM S63845 and 30 μM Q-VD-OPh. Experiment performed with 4

independent repeats. Significance (coloured dots) determined using Students T Test. Plot generated in R studio. B) Pie chart of ubiquitylated peptides categorised into mitochondrial compartments. Categorisation of peptides was performed using MitoCarta 3.0, UniProt and ProteinAtlas. C) Cellular distribution of all hits from the isolated ubiquitin remnant-containing peptides. Categorisation using MitoCarta3.0, UniProt and ProteinAtlas. D) GO-term cellular compartment analysis of proteins with increased ubiquitylation after MOMP. Graphs shows the top 10 most significant hits.

Figure 3 K63-linked ubiquitylation on mitochondria after MOMP

A) SVEC4-10 cells treated with for 1 or 3 hours with 10 μM ABT-737, 10 μM S63845 and 30 μM Q-VD-OPh. Mitochondria were isolated using digitonin fractionation buffer and antibodies against pan-ubiquitin (UBCJ2), K63- and K48-specific ubiquitin were used. Blots representative for 3 independent experiments. B) U2OS EMPTY^{CRISPR} and. BAX/BAK^{CRISPR} cells treated with 10 μM ABT-737, 2 μM S63845 and 20 μM Q-VD-OPh for 3 hours. Stained for K63-ubiquitin and COXIV. Images are maximum projections of Z-stacks with a scale of 20 μm and are representative of 3 independent experiments. C) Quantification of D showing the percentage of cells with mitochondrial localised K63-ubiquitin puncti. Statistics performed using two-way ANOVA with Tukey correction. D) SVEC4-10 cells expressing doxycycline-inducible K63 or M1-UBDs. Cells were treated for 1 hour with 10 μM ABT-737, 10 μM S63845 and 30 μM Q-VD-OPh. Images are representative of 3 independent experiments with a scale bar of 50 μm. E) Quantification of D showing the percentage of SVEC 4-10 cells with mitochondrial localised GFP-UBDs. Also includes the quantification of U2OS cells expressing doxycycline-inducible K63- or M1-UBDs treated for 3 hours with 10 μM

819 ABT-737, 2 μM S63845 and 20 μM Q-VD-OPh. Statistics were performed using
820 multiple unpaired t-tests. ** $p < 0.01$, *** $p < 0.001$. **** $p < 0.0001$.
821
822 **Figure 4 Ubiquitin-dependent recruitment of NEMO to mitochondria is essential**
823 **for NF-κB activation after MOMP**
824 A) U2OS EMPTY^{CRISPR} and BAX/BAK^{CRISPR} cells expressing GFP-NEMO were treated
825 for 3 hours with 10 μM ABT-737, 2 μM S63845 and 20 μM Q-VD-OPh. Cells were
826 immunostained for COXIV. Scale bar is 20 μm. Images are maximum projections of
827 Z-stacks and are representative for 3 independent experiments. B) Quantification of A
828 showing the percentage of cells with mitochondrial localised GFP-NEMO puncti. C)
829 SVEC4-10 cells expressing GFP-NEMO were pre-treated for 1 hour with 2 μM TAK-
830 243 followed by 1 hour treatment of 10 μM ABT-737, 10 μM S63845, 30 μM Q-VD-
831 OPh with or without 2 μM TAK-243. Cells were immunostained for TOM20 and
832 ubiquitin (FK2). Scale bar is 50 μm and images are representative for 3 independent
833 experiments. D) Quantification of C showing the percentage of cells with mitochondrial
834 localised GFP-NEMO and ubiquitin puncti. E) U2OS cells expressing GFP-NEMO,
835 GFP-NEMOD311N or GFP-NEMOΔZF were treated for 3 hours with 10 μM ABT-737,
836 2 μM S63845 and 20 μM Q-VD-OPh. Cells were immunostained for TOM20 and DAPI.
837 Scale bar is 20 μm and images are representative for 3 independent experiments. F)
838 Quantification of E showing the percentage of cells with mitochondrial translocation of
839 GFP-NEMO. G) Parental SVEC4-10 cells and SVEC4-10 cells expressing GFP-
840 NEMO, GFP-NEMOD311N or GFP-NEMOΔZF were treated for 1 hour with 10 μM
841 ABT-737, 10 μM S63845 and 30 μM Q-VD-OPh. Cells were immunostained for p65
842 and DAPI. Scale bar is 50 μm and images are representative for 3 independent
843 experiments. H) Quantification of G showing the GFP+ cells with nuclear translocation

of p65. Statistics are performed using two-way ANOVA with Tukey correction. ** p < 0.01, *** p < 0.001. **** p < 0.0001.

Figure 5 Ubiquitylation-induced inflammation after MOMP is independent of established mitochondrial E3 ligases

A) Lysates of U2OS, SVEC4-10 and SHSHY-5Y cells were blotted for Parkin and actin. B) SVEC4-10 EMPTY^{CRISPR} and PINK1^{CRISPR} cells expressing GFP-NEMO were treated for 1 hour with 10 μM ABT-737, 10 μM S63845 and 30 μM Q-VD-OPh. Cells were immunostained for TOM20. Images are representative for 3 independent experiments with a scale bar of 50 μm. C) Quantification of B showing the percentage of cells with mitochondrial translocation of GFP-NEMO. D) SVEC4-10 EMPTY^{CRISPR}, MUL1^{CRISPR}, MARCH5^{CRISPR} and MUL1/MARCH5^{CRISPR} treated for 3 hours with 10 μM ABT-737, 10 μM S63845 and 30 μM Q-VD-OPh. Lysates were blotted for p-IκBα, IκBα, MARCH5 and actin. Blots are representative of 3 independent experiments. KO-scores of MUL1 and MARCH5 are calculated via ICE analysis. E) SVEC4-10 EMPTY^{CRISPR} and MUL1/MARCH5^{CRISPR} cells expressing GFP-NEMO treated for 1 hour with 10 μM ABT-737, 10 μM S63845 and 30 μM Q-VD-OPh. Cells were immunostained for ubiquitin (UBCJ2) and TOM20. Images are representative for 3 independent experiments with a scale bar of 50 μm. F) Quantification of E showing the percentage of cells with mitochondrial localisation of GFP-NEMO and ubiquitin. G) SVEC4-10 EMPTY^{CRISPR} and XIAP^{CRISPR} cells expressing GFP-NEMO were treated with 10 μM ABT-737, 10 μM S63845 and 30 μM Q-VD-OPh for 1 hour. Cells were immunostained for ubiquitin (FK2) and TOM20 Images are representative for 3 independent experiments with a scale bar of 50 μm. H) Quantification of G showing the percentage of cells with mitochondrial localisation of GFP-NEMO and ubiquitin.

Statistics were performed using two-way ANOVA with Tukey correction. **** $p < 0.0001$.

Figure 6 Mitochondrial ubiquitylation and inflammation occurs upon loss of mitochondrial outer membrane integrity

A) SVEC4-10 cells expressing GFP-NEMO were treated for 3 hours with 10 μM ABT-737, 10 μM S63845 and 30 μM Q-VD-OPh or 2.5 μM raptinal and 30 μM Q-VD-OPh. Cells were immunostained for ubiquitin (FK2) and TOM20. Images are representative of 2 independent experiments displayed with a 50 μm scale bar. B) Quantification of A showing the percentage of cells with mitochondrial localisation of GFP-NEMO and ubiquitin. Percentages of cells with mitochondrial localisation of GFP-NEMO was determined in 3 independent experiments, while mitochondrial localisation of ubiquitin was determined in 2 independent experiments. C) SVEC4-10 EMPTY^{CRISPR} and BAX/BAK^{CRISPR} cells were treated for 3 hours with 10 μM ABT-737, 10 μM S63845 and 30 μM Q-VD-OPh or 2.5 μM raptinal and 30 μM Q-VD-OPh. Cells were immunostained stained for p65 and DAPI. Images are representative of 3 independent experiments and are shown with a 50 μm scale bar. D) Quantification of B showing the percentage of cells with nuclear translocation of p65. E) SVEC4-10 cells treated for 3 hours with 10 μM ABT-737, 10 μM S63856 and 30 μM Q-VD-OPh or 2.5 μM raptinal and 30 μM Q-VD-OPh. Expression of *Kc*, *Tnf* and *Actin* were validated using RT-qPCR. Graphs are representative for 3 independent experiments. Statistics were performed using Dunnett correction. **** $p < 0.0001$.

Supplemental Figure 1 Ubiquitylation of mitochondria is dependent on MOMP by BAX/BAK pores, but independent of caspase activity

A) Lysates from U2OS EMPTY^{CRISPR} and BAX/BAK^{CRISPR} cells were blotted for BAX, BAK and Actin. B) U2OS EMPTY^{CRISPR} and BAX/BAK^{CRISPR} cells were treated with 10 μM ABT-737, 2 μM S63845 with or without 20 μM Q-VD-OPh. Cell death was monitored using Sytox Green inclusion normalised to starting confluence. Graph is representative for 3 independent experiments. C) SVEC4-10 EMPTY^{CRISPR} and BAX/BAK^{CRISPR} cells were treated for 1 hour with 10 μM ABT-737, 10 μM S63845 and 30 μM Q-VD-OPh. Mitochondria were isolated using digitonin fractionation buffer and blotted for ubiquitin (UBCJ2), BAX, BAK, HSP60 and actin. Blots are representative for 3 independent experiments. D) SVEC4-10 cells were treated for 1 hour with 10 μM ABT-737, 10 μM S63845 with or without 30 μM Q-VD-OPh. Mitochondria were isolated using digitonin fractionation buffer and lysates were blotted for ubiquitin (UBCJ2), HSP60 and actin. Blots are representative for 3 independent experiments.

Supplemental Figure 2 Mitochondrial ubiquitylation and GFP-NEMO translocation can be blocked by E1 inhibition and is independent of neddylation

A) SVEC4-10 cells pre-treated with 2 μM TAK-243 for 1 hour followed by additional 1 hour treatment with 10 μM ABT-737, 10 μM S63845 and 30 μM Q-VD-OPh with or without the additional of 2 μM TAK-243. Blots are representative for 4 independent experiments. B) SVEC4-10 cells pre-treated with 1 μM MLN4924 (NAE inhibitor) for 1 hour followed by additional 1 hour treatment with 10 μM ABT-737, 10 μM S63845 and 30 μM Q-VD-OPh with or without 1 μM MLN4924. Blots are representative for 2 independent experiments. C) SVEC4-10 cells expressing GFP-NEMO pre-treated with 1 μM MLN4924 for 1 hour followed by additional 1 hour treatment with 10 μM ABT-

737, 10 μM S63845 and 30 μM Q-VD-OPh with or without 1 μM MLN4924. Cells were immunostained for TOM20 and DAPI. Images are representative for 3 independent experiments and are shown with a 50 μm scale bar. D) Quantification of C showing the percentage of cells with mitochondrial translocation of GFP-NEMO. Statistics were performed using two-way ANOVA with Tukey correction. **** $p < 0.0001$.

Supplemental Figure 3 Loss of NEMO cannot be rescued during CICD by expressing non-ubiquitin binding mutants of NEMO

A) MEF *Tnf*$^{-/-}$ *Hoip*$^{+/+}$ and *Tnf*$^{-/-}$ *Hoip*$^{+/+}$ expressing GFP-NEMO were treated for 3 hours with 10 μM ABT-737, 5 μM S63845 and 30 μM Q-VD-OPh. Cells were immunostained for TOM20 and DAPI. Images are representative of 3 independent experiments. B) Quantification of A showing the percentage of cells with mitochondrial translocation of GFP-NEMO. Statistics were performed using two-way ANOVA with Tukey correction. C) Validation of SVEC4-10, SVEC4-10 GFP-NEMO and SVEC4-10 GFP-D311N cells transfected with NTC or siNEMO. Lysates were blotted for NEMO and α-tubulin. D) SVEC4-10, SVEC4-10 GFP-NEMO and SVEC4-10 GFP-D311N cells transfected with NTC or siNEMO were treated for 1 hour with 10 μM ABT-737, 10 μM S63845 and 30 μM Q-VD-OPh. Cells were immunostained for p65 and DAPI. Images are representative of 2 independent experiments. E) Quantification of D showing the percentage of cells with nuclear translocation of p65. **** $p < 0.0001$.

Supplemental Figure 4 Validation of PINK1^{CRISPR}, NIK^{CRISPR}, MUL1MARCH5^{CRISPR} and XIAP^{CRISPR} knock-out cell lines

A) Validation of PINK1 knock-out in SVEC4-10 cells with or without GFP-NEMO expression using genomic PCR and ICE (interference of CRISPR edits) analysis. B)

SVEC4-10 EMPTY^{CRISPR} and PINK1^{CRISPR} cells expressing YFP-Parkin were treated for 1 hour with 10 μM ABT-737, 10 μM S63845 and 30 μM QVD for 3 hours with 10 μM CCCP. Mitochondria were immunostained with HSP60 and DAPI. Images are representative of 2 independent experiments and displayed with 50 μm scale bar. C) Validation of MUL1 knock-out in SVEC4-10 MUL1MARCH5^{CRISPR} cells using genomic PCR and ICE analysis. D) Validation of MARCH5 knock-out in SVEC4-10 MUL1MARCH5^{CRISPR} cells using genomic PCR and ICE analysis. E) Validation of SVEC4-10 XIAP^{CRISPR} cells with and without GFP-NEMO expression using western blot. Lysates were blotted for XIAP and actin. F) *Tnf*, *Kc,* and *Ccl5* expression of SVEC4-10 EMPTY^{CRISPR} and XIAP^{CRISPR} cells treated with 10 μM ABT-737, 10 μM S63845 and 30 μM QVD for 3 hours. Graph is representative for 3 independent experiments.

Supplemental Figure 5 Raptinal induces cell death independent of mitochondrial permeabilization by BAX and BAK

A) EMPTY^{CRISPR} and BAX/BAK^{CRISPR} validation of SVEC4-10 cells and SVEC4-10 cells expressing GFP-NEMO. Lysates for blotted for BAX, BAK and α-tubulin. B) SVEC4-10 EMPTY^{CRISPR} and SVEC4-10 BAX/BAK^{CRISPR} cells treated with 10 μM ABT-737 and 10 μM S63845 or treated with 2.5 or 10 μM raptinal. Caspase-dependency of death was assessed using 30 μM Q-VD-OPh. Cell viability was measured using Sytox Green exclusion. Graphs are representative of 2 independent experiments and display the mean and SEM of 2 replicates. Statistics performed using two-way ANOVA with Tukey correction. *** $p < 0.001$, **** $p < 0.0001$.

Supplemental Table 1

Intramitochondrial localisation of proteins found to be ubiquitylated upon MOMP

966

967

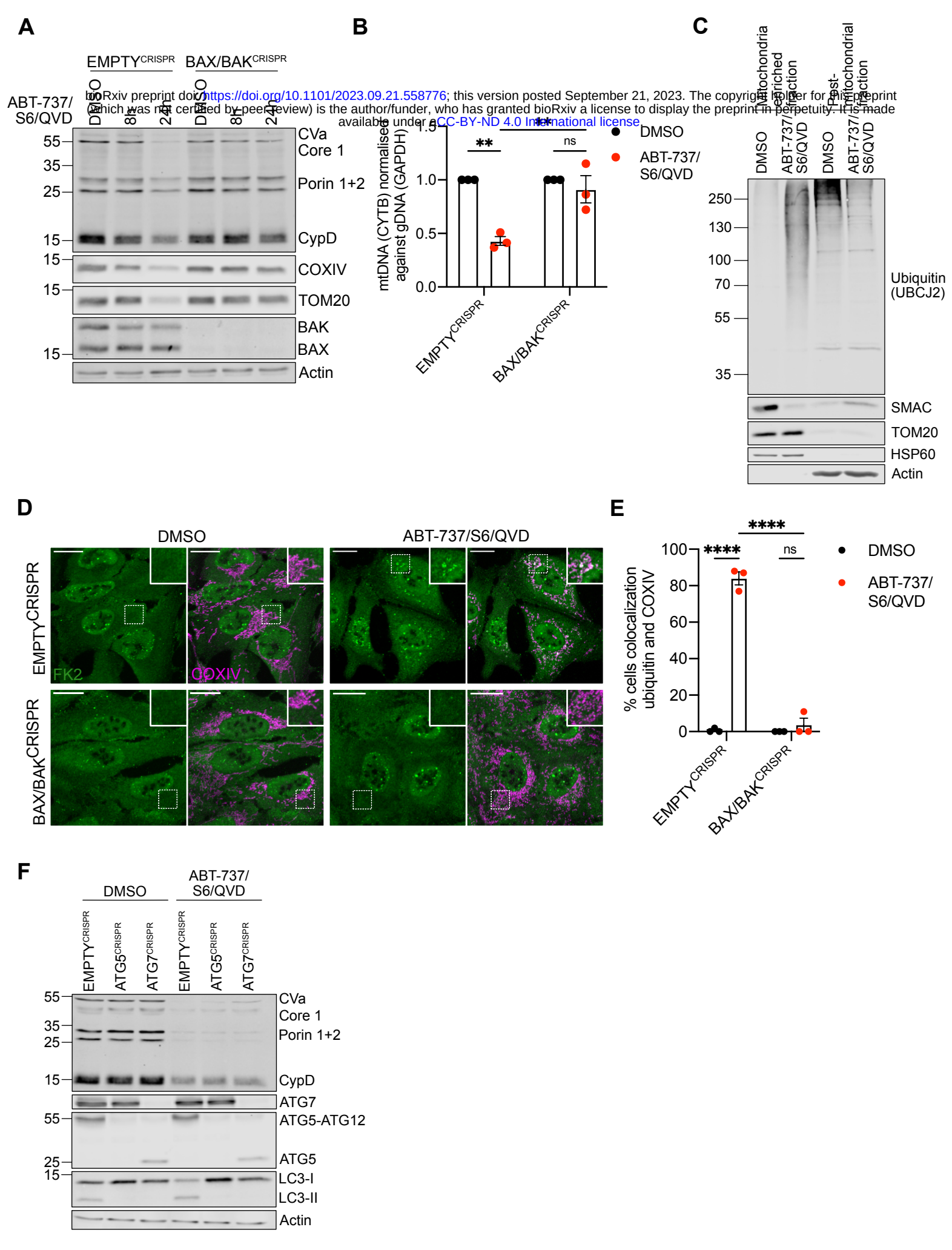

Figure 1

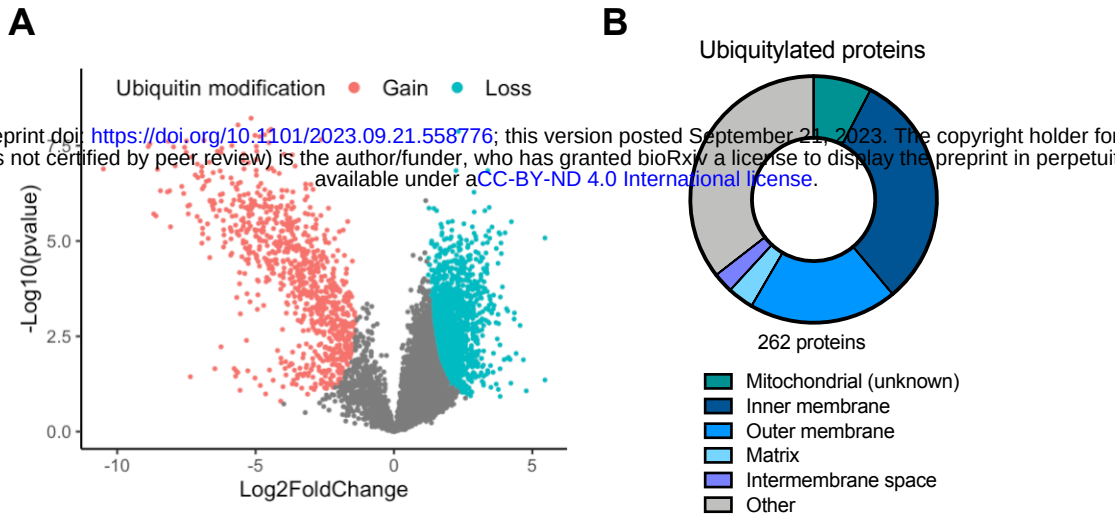

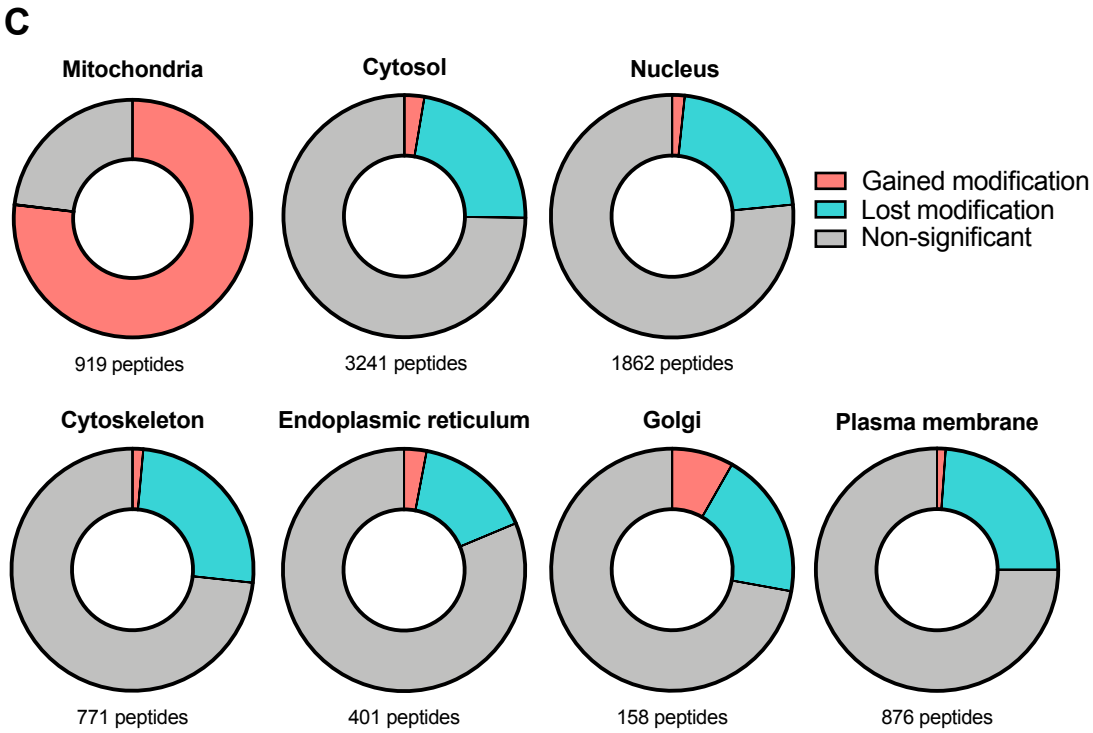

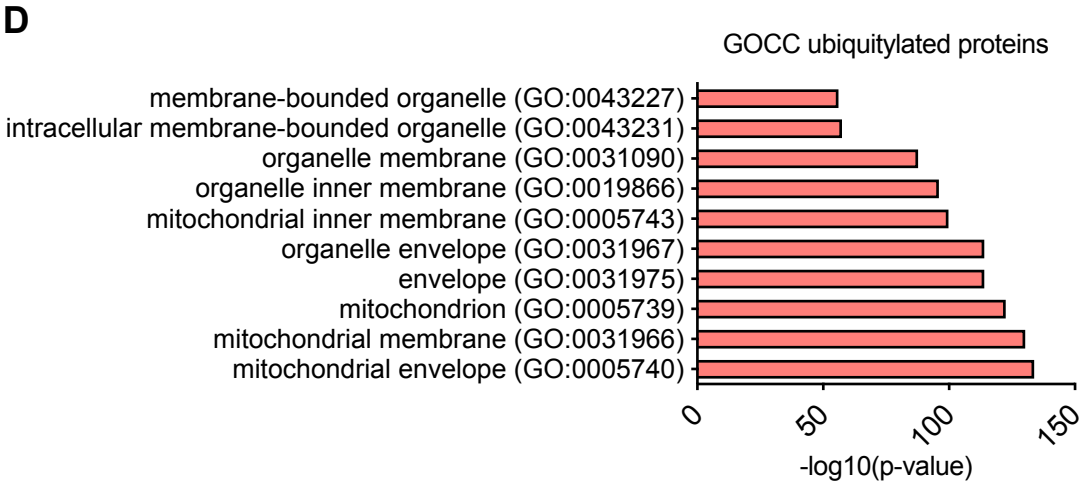

Figure 2

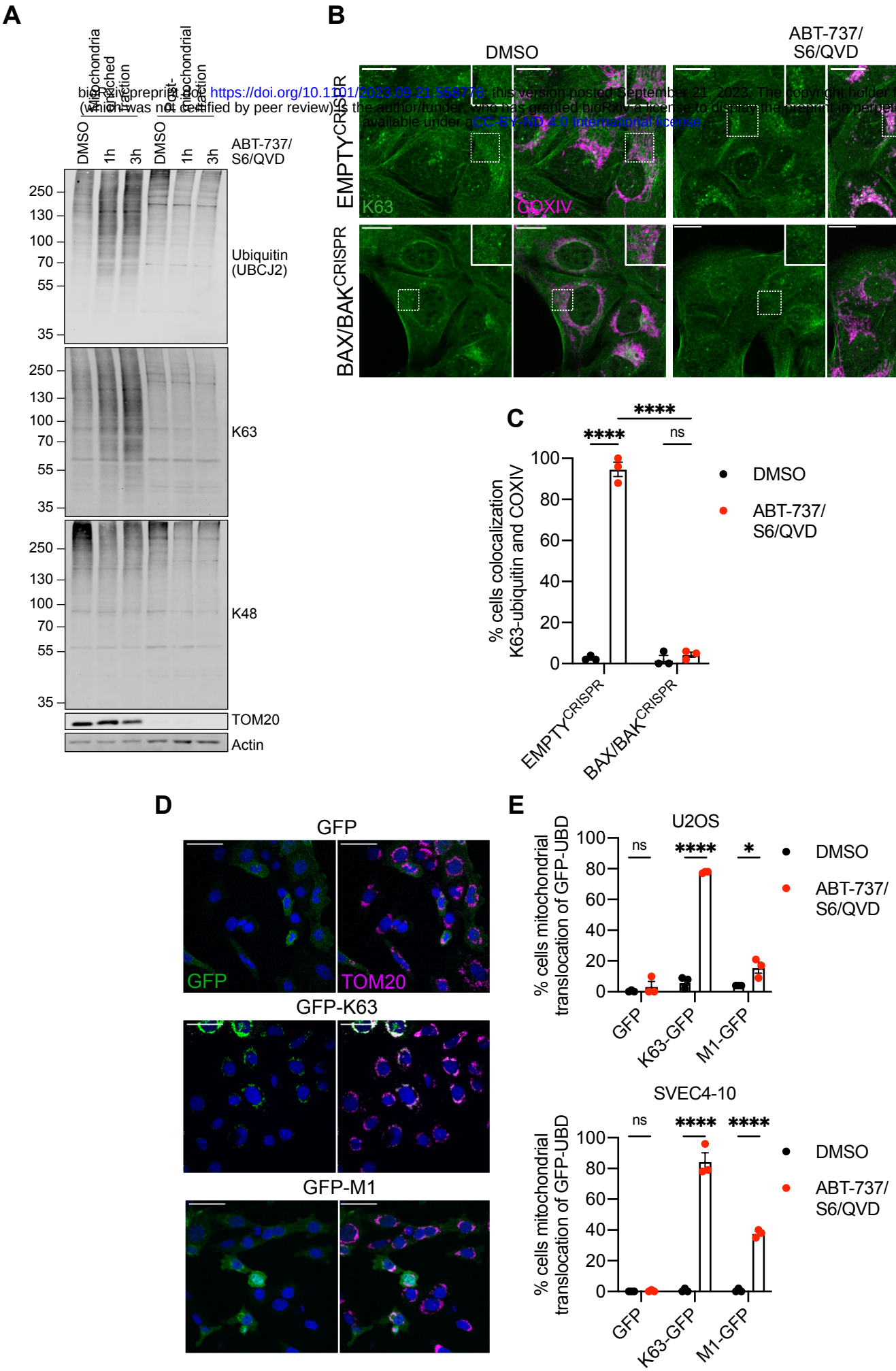

Figure 3

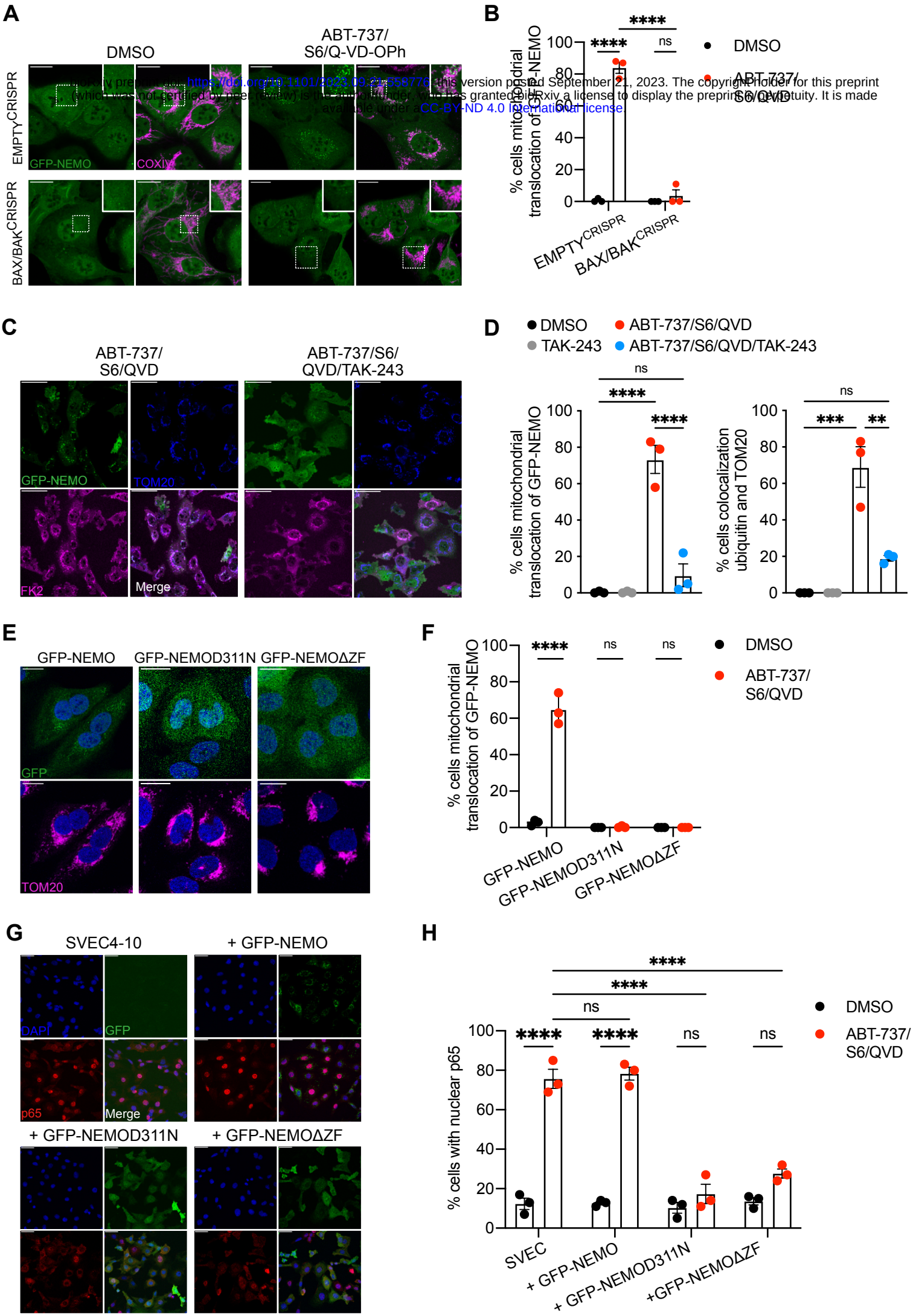

Figure 4

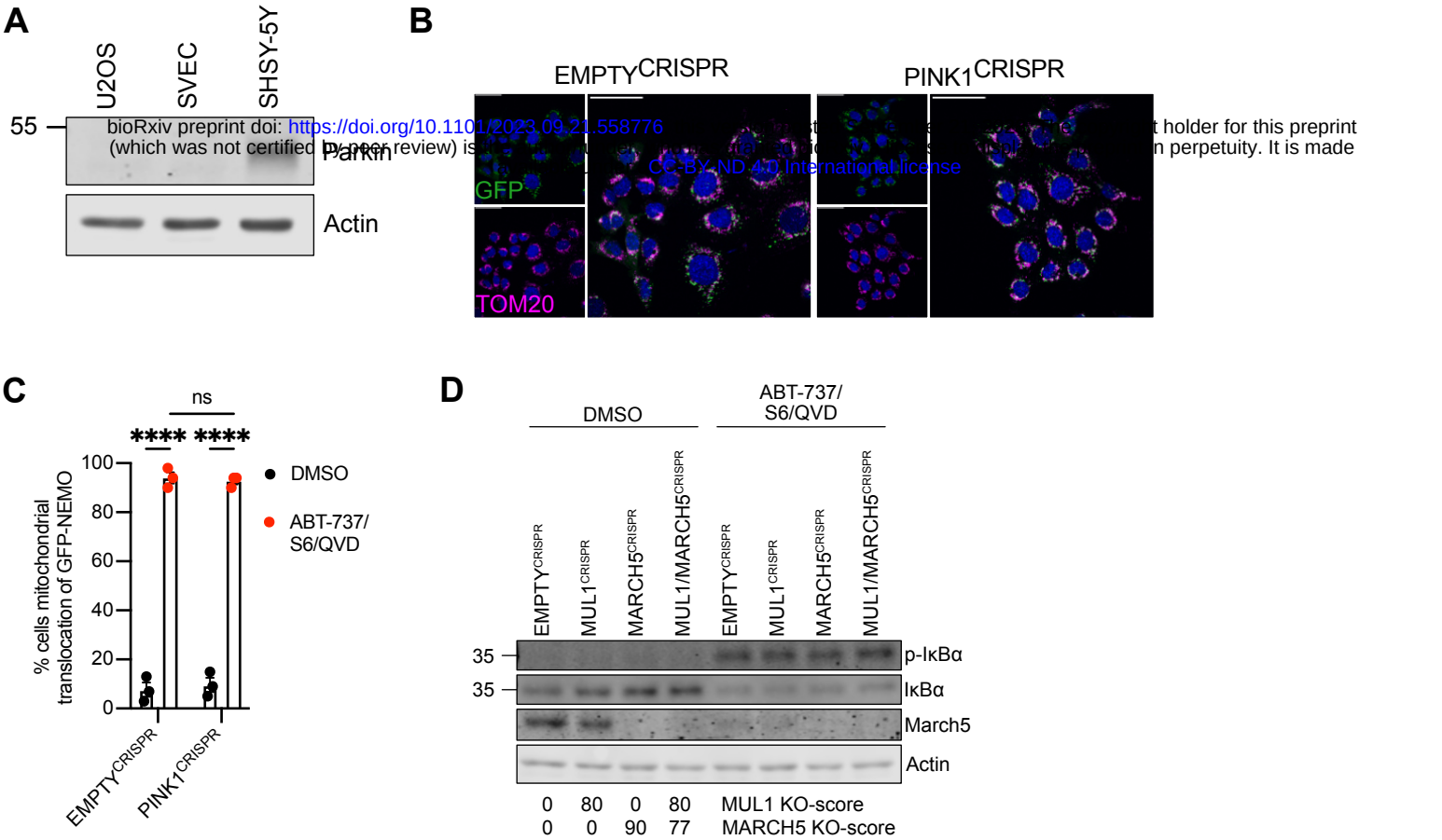

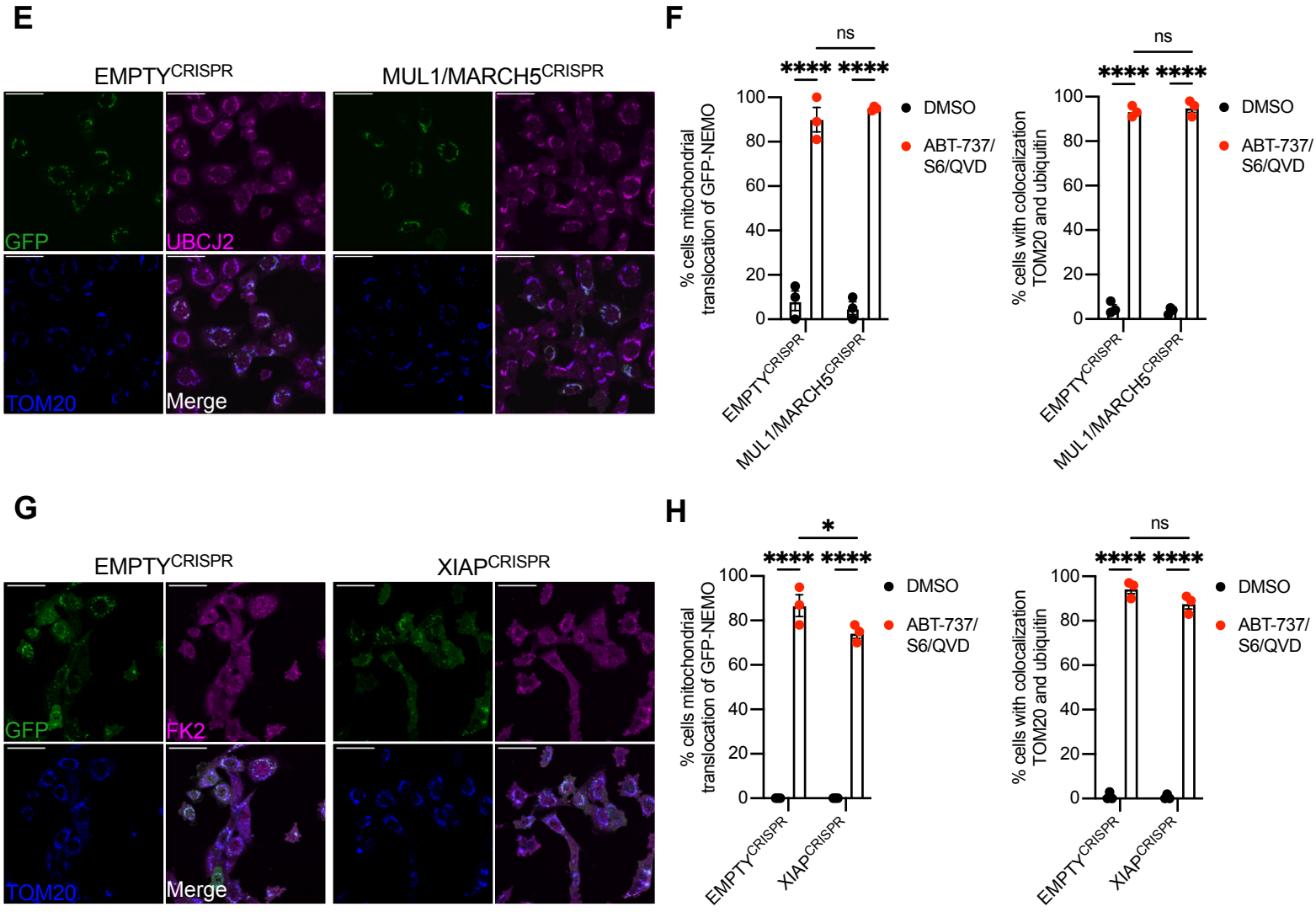

Figure 5

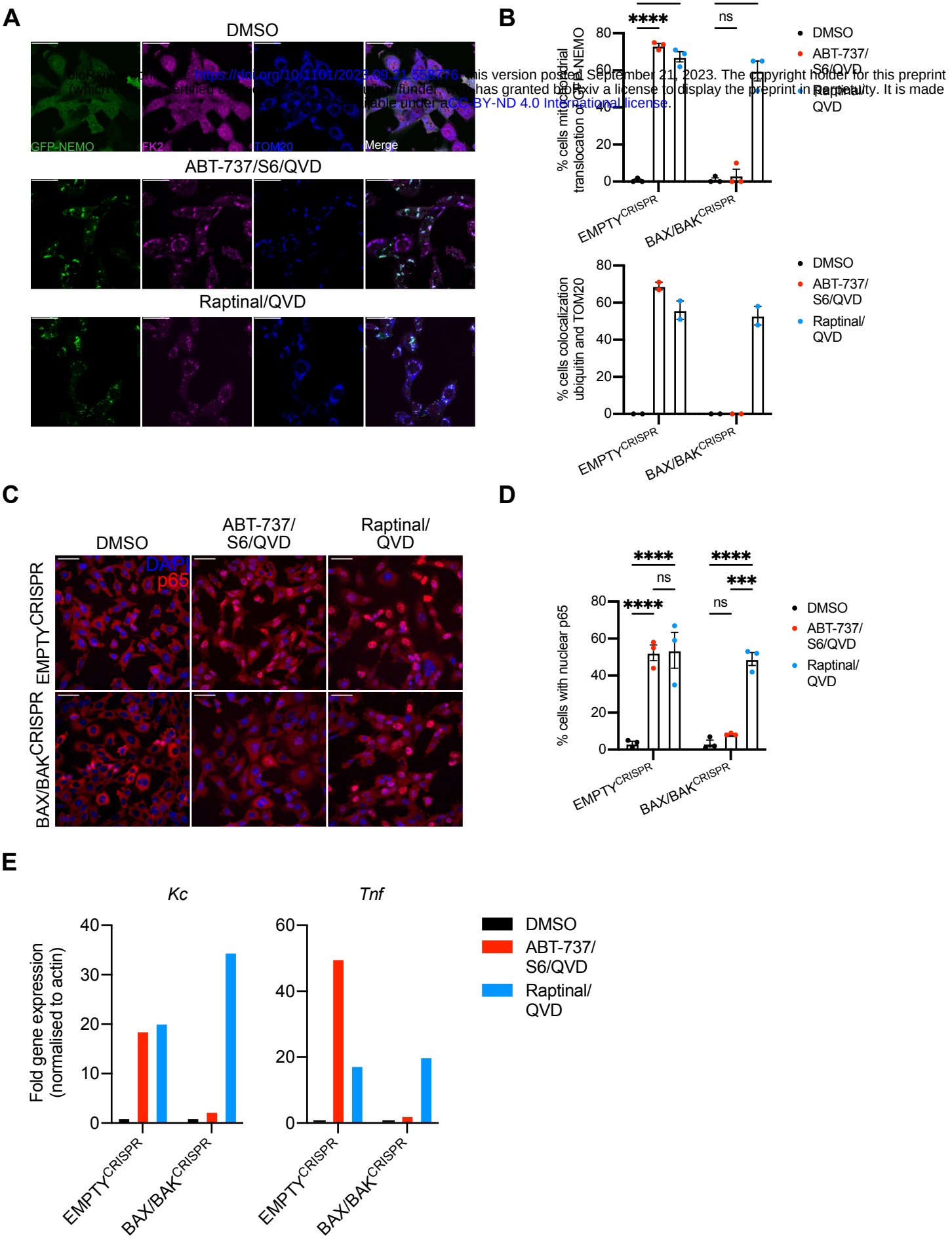

Figure 6

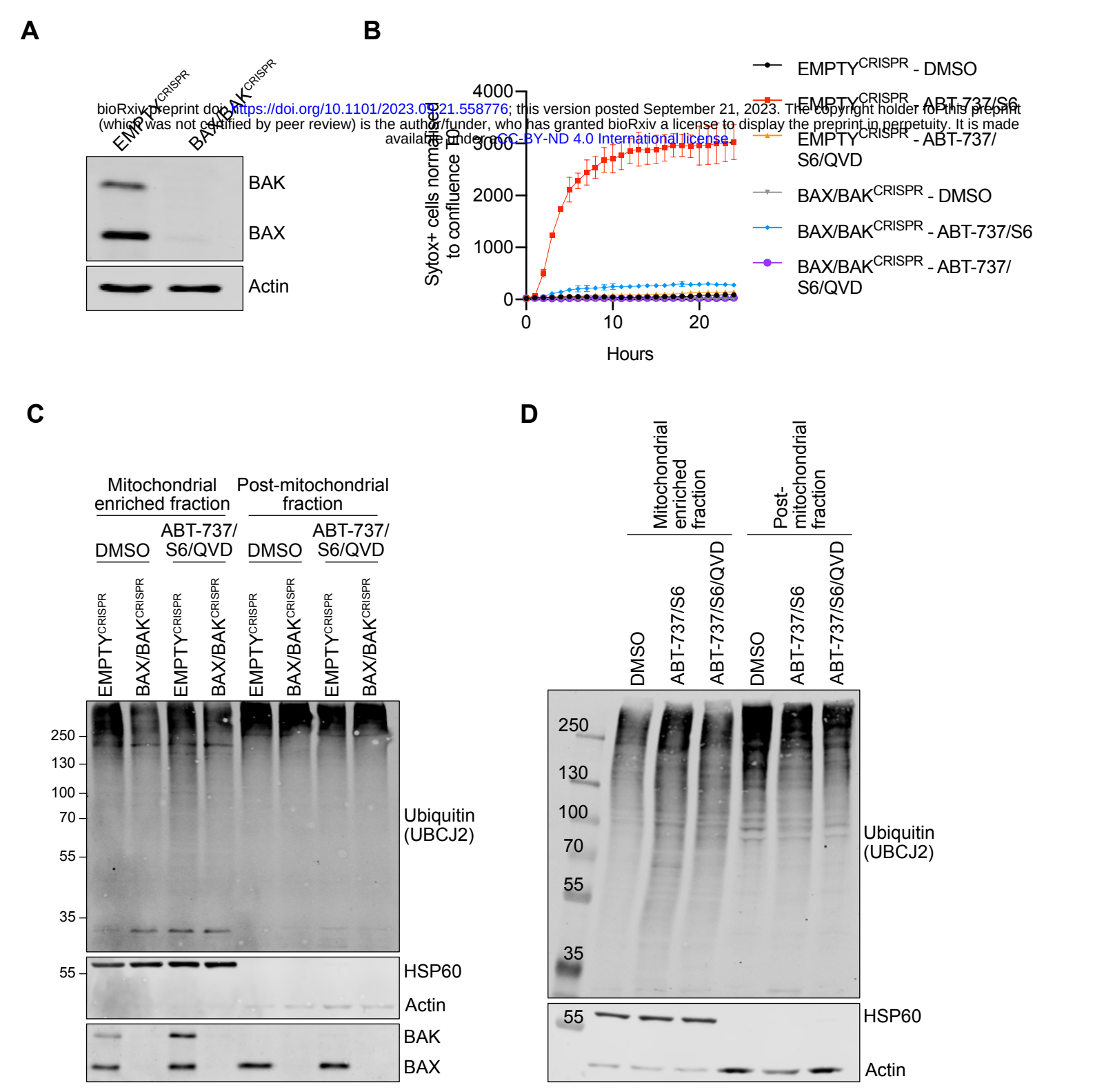

Supplemental Figure 1

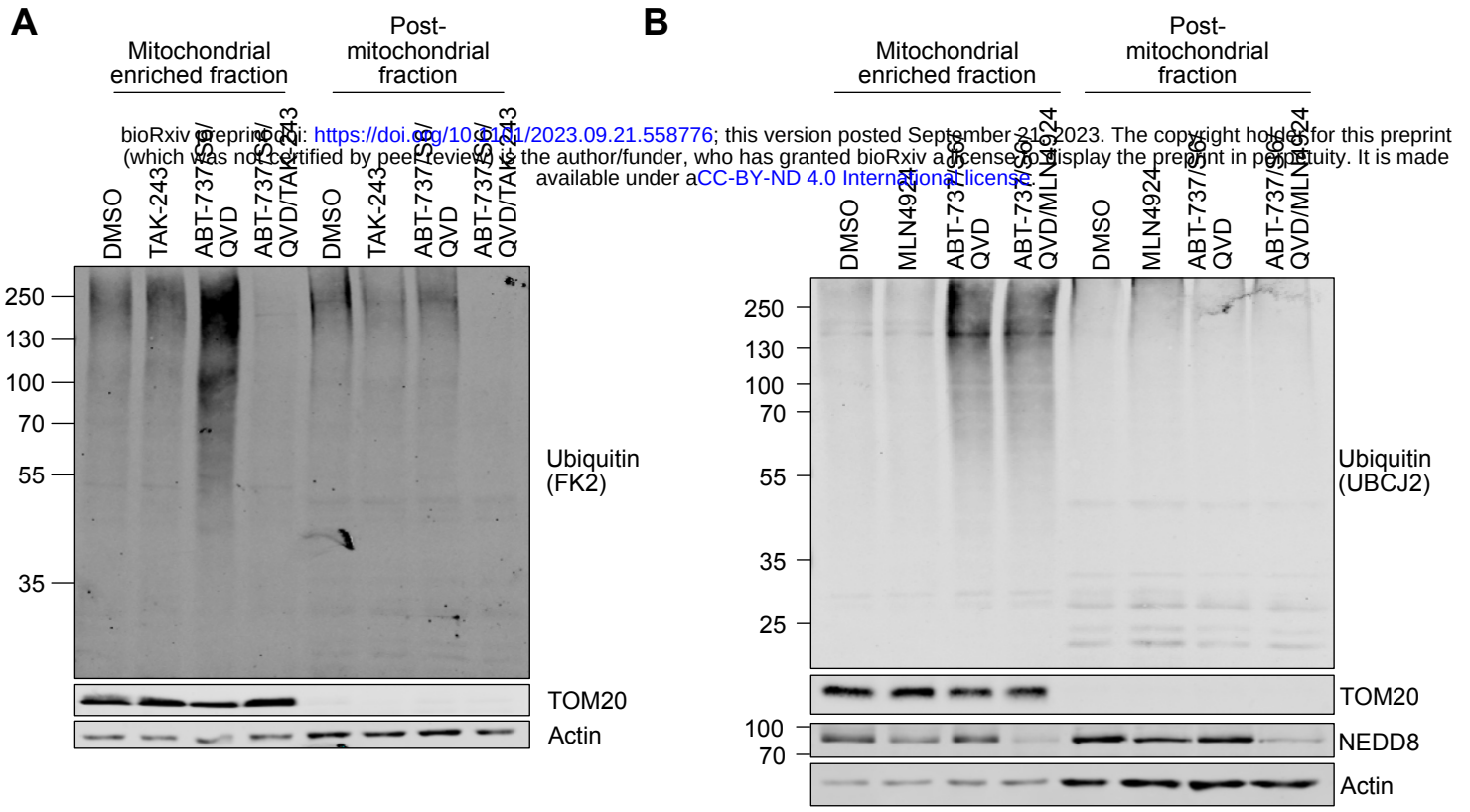

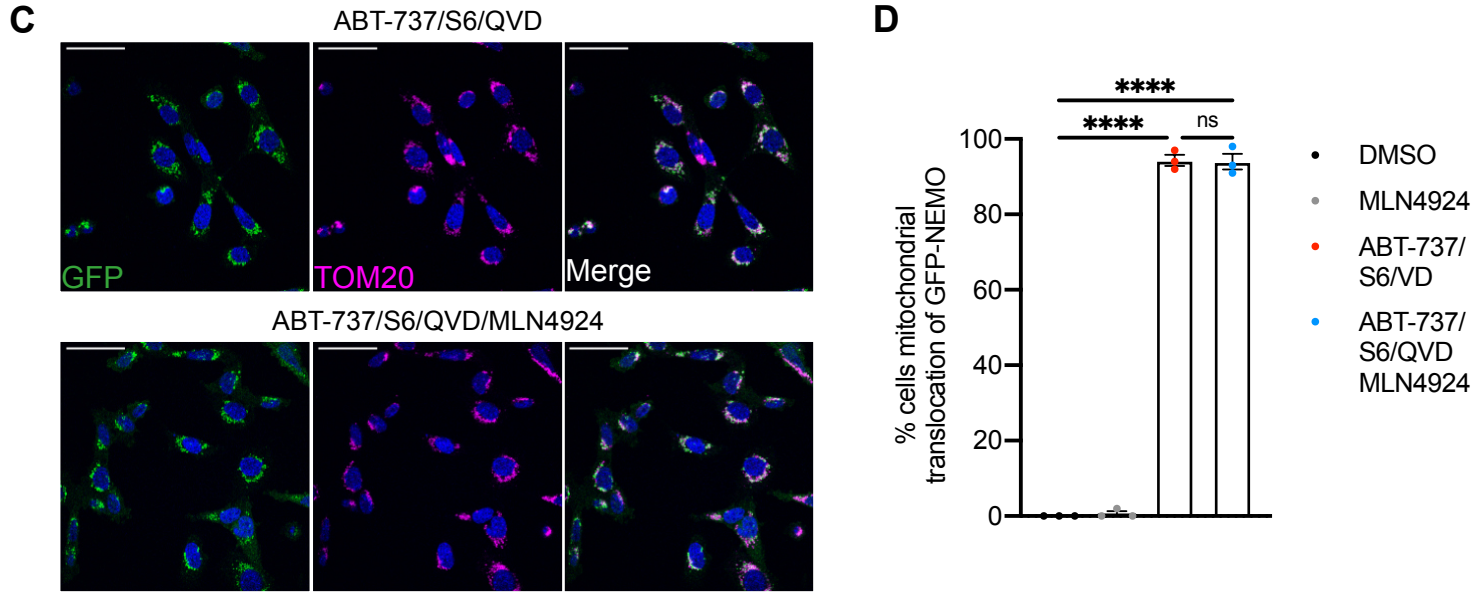

Supplemental Figure 2

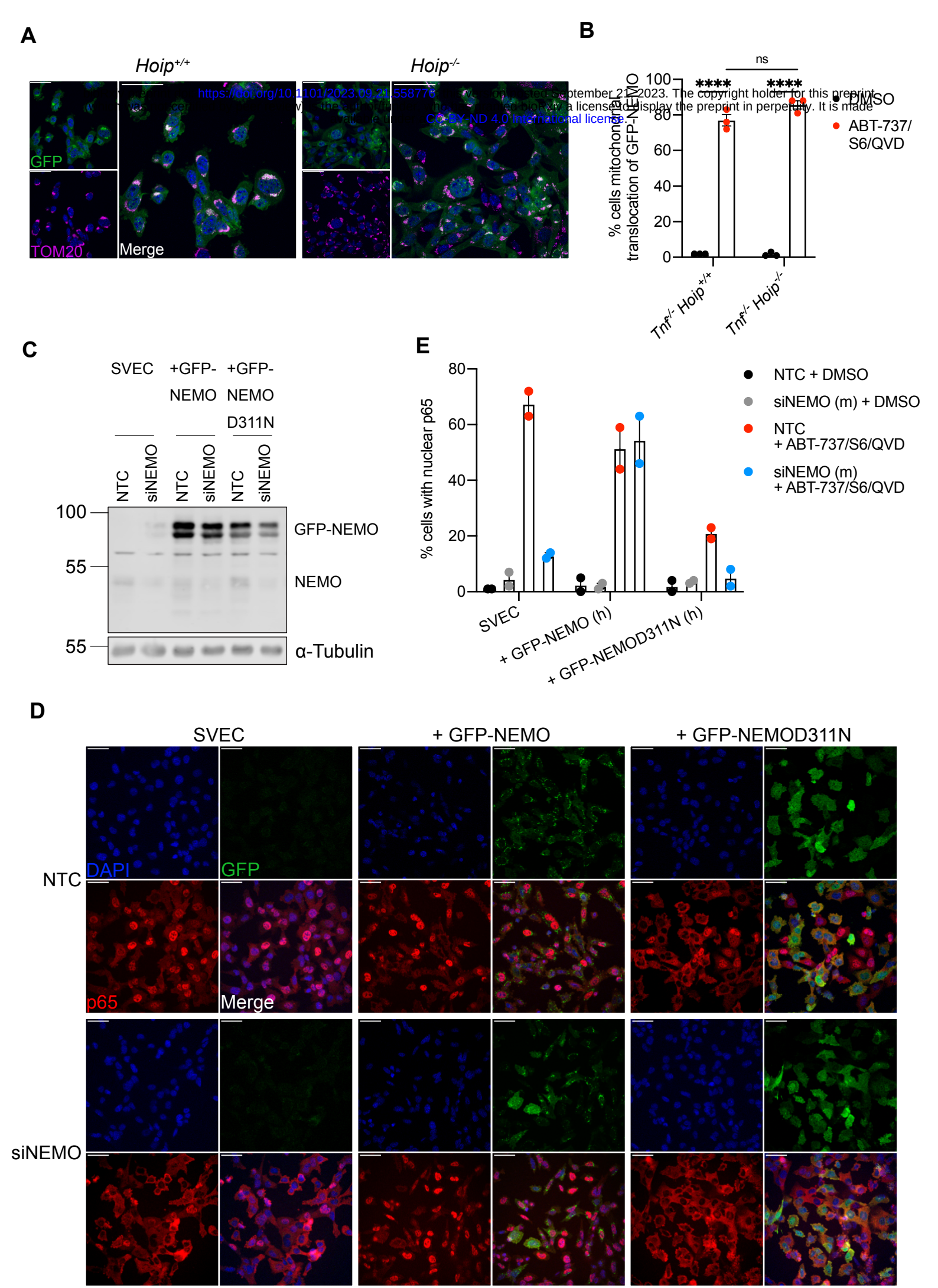

Supplemental Figure 3

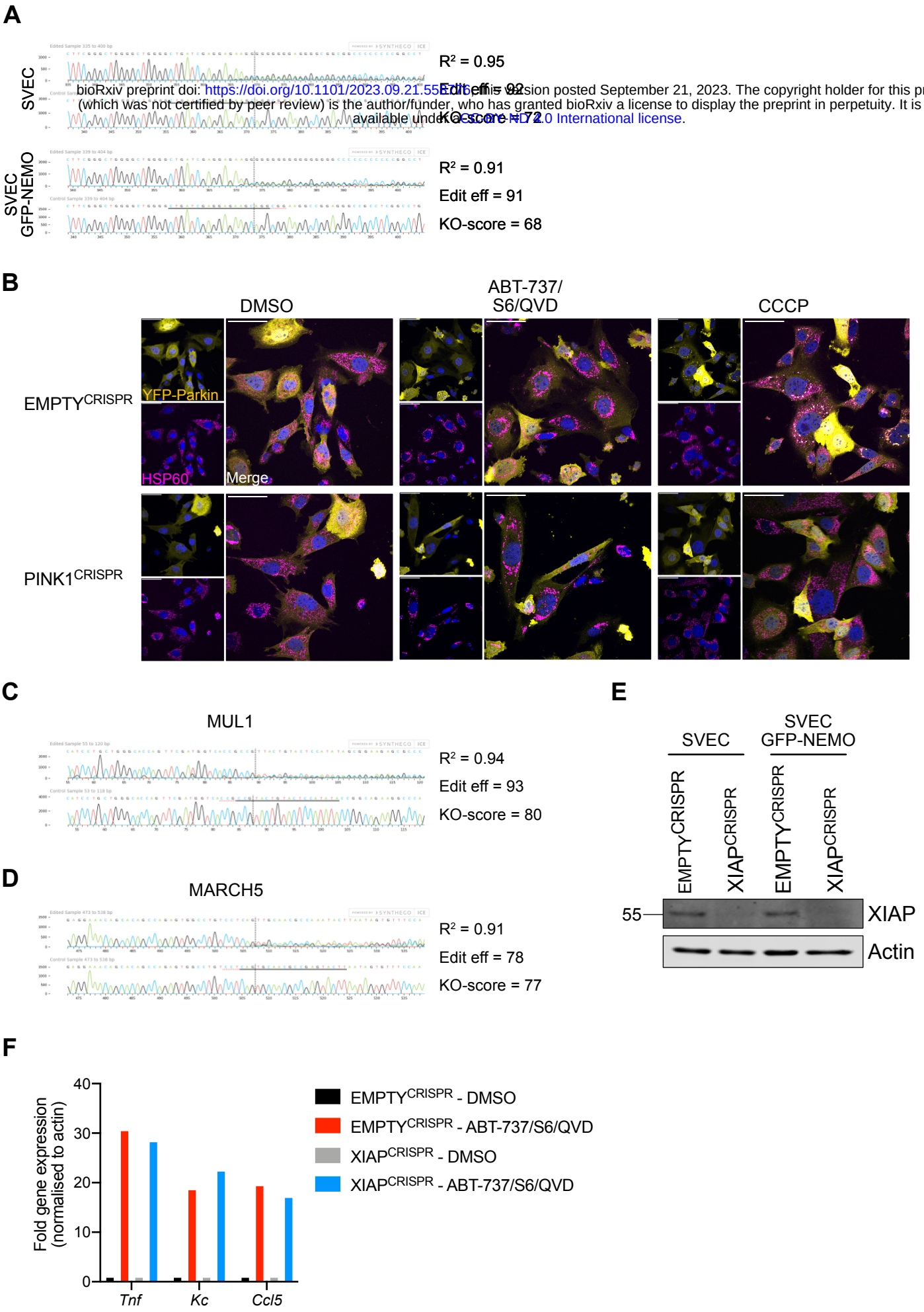

Supplemental Figure 4

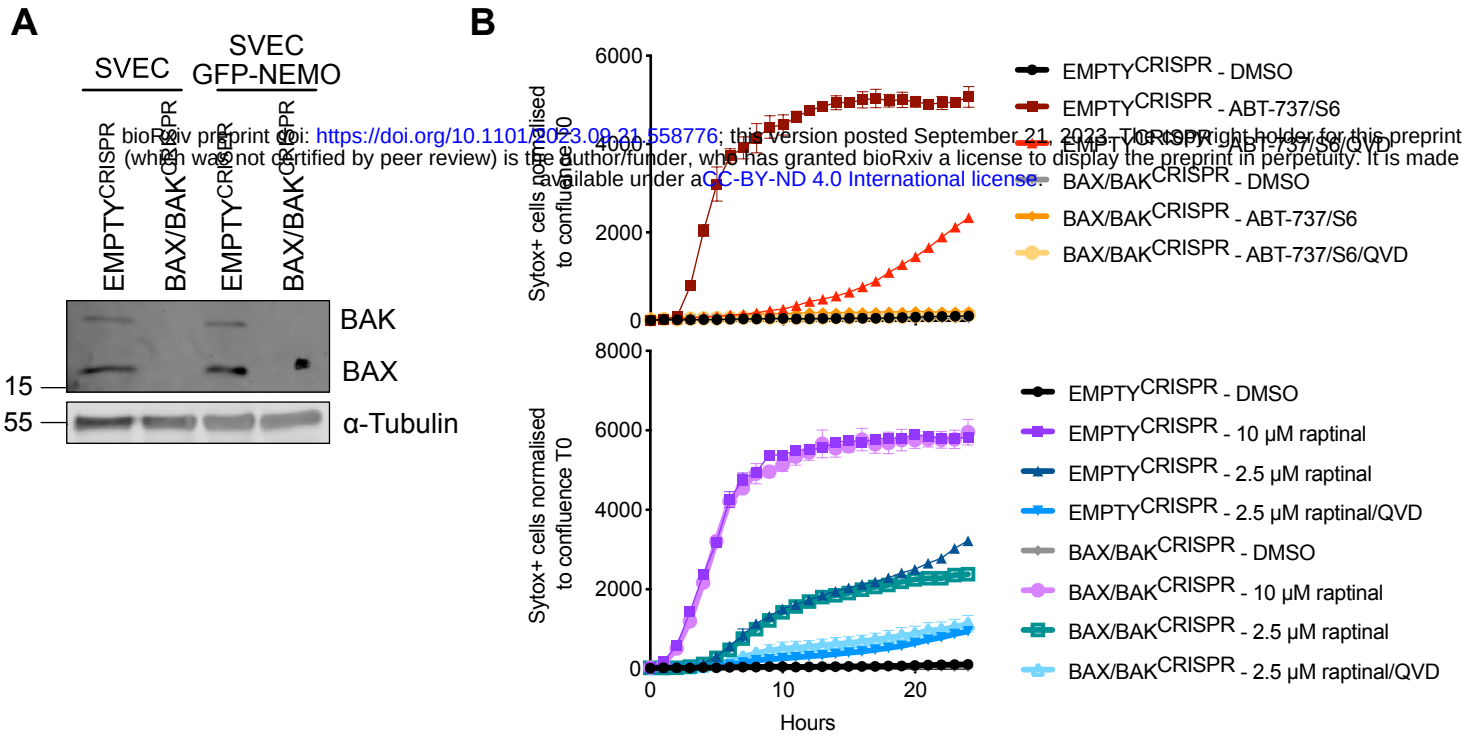

Supplemental Figure 5

Gene names	Student's T-test Significant	Localization	Source
Acad11	Ubiquitylated upon MOMP	Inner Mitochondrial Membrane	Mitocarta3.0
Acot9;Acot10	Ubiquitylated upon MOMP	Inner Mitochondrial Membrane	Mitocarta3.0
Agk	Ubiquitylated upon MOMP	Inner Mitochondrial Membrane	Mitocarta3.0
Agpat5	Ubiquitylated upon MOMP	Outer Mitochondrial Membrane	Mitocarta3.0
Aifm1	Ubiquitylated upon MOMP	Inner Mitochondrial Membrane	Mitocarta3.0
Ak2	Ubiquitylated upon MOMP	Mitochondrial Intermembrane Space	Mitocarta3.0
Akap1	Ubiquitylated upon MOMP	Outer Mitochondrial Membrane	Mitocarta3.0
Apool	Ubiquitylated upon MOMP	Inner Mitochondrial Membrane	Mitocarta3.0
Armc10	Ubiquitylated upon MOMP	Outer Mitochondrial Membrane	Mitocarta3.0
Armcx3	Ubiquitylated upon MOMP	Outer Mitochondrial Membrane	Mitocarta3.0
Atad1	Ubiquitylated upon MOMP	Outer Mitochondrial Membrane	Mitocarta3.0
Atad3	Ubiquitylated upon MOMP	Inner Mitochondrial Membrane	Mitocarta3.0
Atp5b	Ubiquitylated upon MOMP	Inner Mitochondrial Membrane	Mitocarta3.0
Atp5i	Ubiquitylated upon MOMP	Inner Mitochondrial Membrane	Mitocarta3.0
Bak1	Ubiquitylated upon MOMP	Outer Mitochondrial Membrane	Mitocarta3.0
Bax	Ubiquitylated upon MOMP	Outer Mitochondrial Membrane	Mitocarta3.0
Bcl2l1	Ubiquitylated upon MOMP	Outer Mitochondrial Membrane	Mitocarta3.0
Bcl2l13	Ubiquitylated upon MOMP	Outer Mitochondrial Membrane	Mitocarta3.0
Bnip3l	Ubiquitylated upon MOMP	Outer Mitochondrial Membrane	Mitocarta3.0
Card19	Ubiquitylated upon MOMP	Unknown mitochondrial localisation	Uniprot
Ccdc127	Ubiquitylated upon MOMP	Unknown mitochondrial localisation	Mitocarta3.0
Ccdc51	Ubiquitylated upon MOMP	Inner Mitochondrial Membrane	Mitocarta3.0
Ccdc58	Ubiquitylated upon MOMP	Mitochondrial Intermembrane Space	Mitocarta3.0
Chchd3	Ubiquitylated upon MOMP	Inner Mitochondrial Membrane	Mitocarta3.0
Chchd4	Ubiquitylated upon MOMP	Mitochondrial Intermembrane Space	Mitocarta3.0
Chchd6	Ubiquitylated upon MOMP	Inner Mitochondrial Membrane	Mitocarta3.0
Cisd1	Ubiquitylated upon MOMP	Outer Mitochondrial Membrane	Mitocarta3.0
Coa3	Ubiquitylated upon MOMP	Inner Mitochondrial Membrane	Mitocarta3.0
Comtd1	Ubiquitylated upon MOMP	Unknown mitochondrial localisation	Mitocarta3.0
Cox11	Ubiquitylated upon MOMP	Inner Mitochondrial Membrane	Mitocarta3.0
Cox14	Ubiquitylated upon MOMP	Inner Mitochondrial Membrane	Mitocarta3.0
Cox15	Ubiquitylated upon MOMP	Inner Mitochondrial Membrane	Mitocarta3.0
Cox17	Ubiquitylated upon MOMP	Mitochondrial Intermembrane Space	Mitocarta3.0
Cox20	Ubiquitylated upon MOMP	Inner Mitochondrial Membrane	Mitocarta3.0
Cox4i1	Ubiquitylated upon MOMP	Inner Mitochondrial Membrane	Mitocarta3.0
Cox6b1	Ubiquitylated upon MOMP	Inner Mitochondrial Membrane	Mitocarta3.0
Cox6c	Ubiquitylated upon MOMP	Inner Mitochondrial Membrane	Mitocarta3.0
Cox7a2	Ubiquitylated upon MOMP	Inner Mitochondrial Membrane	Mitocarta3.0
Cox7b	Ubiquitylated upon MOMP	Inner Mitochondrial Membrane	Mitocarta3.0
Cpt1a	Ubiquitylated upon MOMP	Outer Mitochondrial Membrane	Mitocarta3.0
Cs	Ubiquitylated upon MOMP	Mitochondrial matrix	Mitocarta3.0
Cyb5b	Ubiquitylated upon MOMP	Outer Mitochondrial Membrane	Mitocarta3.0
Cyb5r1	Ubiquitylated upon MOMP	Unknown mitochondrial localisation	Uniprot
Cyb5r3	Ubiquitylated upon MOMP	Outer Mitochondrial Membrane	Mitocarta3.0
Cyc1	Ubiquitylated upon MOMP	Inner Mitochondrial Membrane	Mitocarta3.0

Dcakd	Ubiquitylated upon MOMP	Unknown mitochondrial localisation	Mitocarta3.0
Dhfr	Ubiquitylated upon MOMP	Unknown mitochondrial localisation	Uniprot
Dhodh	Ubiquitylated upon MOMP	Inner Mitochondrial Membrane	Mitocarta3.0
Diablo	Ubiquitylated upon MOMP	Mitochondrial Intermembrane Space	Mitocarta3.0
Dlat	Ubiquitylated upon MOMP	Mitochondrial matrix	Mitocarta3.0
Dnajc11	Ubiquitylated upon MOMP	Outer Mitochondrial Membrane	Mitocarta3.0
Exog	Ubiquitylated upon MOMP	Inner Mitochondrial Membrane	Mitocarta3.0
Fam162a	Ubiquitylated upon MOMP	Inner Mitochondrial Membrane	Mitocarta3.0
Fam73b	Ubiquitylated upon MOMP	Outer Mitochondrial Membrane	Mitocarta3.0
Fis1	Ubiquitylated upon MOMP	Outer Mitochondrial Membrane	Mitocarta3.0
Fkbp8	Ubiquitylated upon MOMP	Outer Mitochondrial Membrane	Mitocarta3.0
Fundc2	Ubiquitylated upon MOMP	Outer Mitochondrial Membrane	Mitocarta3.0
Ghitm	Ubiquitylated upon MOMP	Inner Mitochondrial Membrane	Mitocarta3.0
Glrx5	Ubiquitylated upon MOMP	Mitochondrial matrix	Mitocarta3.0
Glud1	Ubiquitylated upon MOMP	Mitochondrial matrix	Mitocarta3.0
Gpam	Ubiquitylated upon MOMP	Unknown mitochondrial localisation	Mitocarta3.0
Gpd2	Ubiquitylated upon MOMP	Inner Mitochondrial Membrane	Mitocarta3.0
Gramd4	Ubiquitylated upon MOMP	Unknown mitochondrial localisation	Uniprot
Gsr	Ubiquitylated upon MOMP	Mitochondrial matrix	Mitocarta3.0
Hccs	Ubiquitylated upon MOMP	Mitochondrial Intermembrane Space	Mitocarta3.0
Hk1	Ubiquitylated upon MOMP	Unknown mitochondrial localisation	Uniprot
Hk2	Ubiquitylated upon MOMP	Unknown mitochondrial localisation	Uniprot
Hsdl1	Ubiquitylated upon MOMP	Unknown mitochondrial localisation	Mitocarta3.0
Hspd1	Ubiquitylated upon MOMP	Unknown mitochondrial localisation	Mitocarta3.0
Htra2	Ubiquitylated upon MOMP	Inner Mitochondrial Membrane	Mitocarta3.0
Immt	Ubiquitylated upon MOMP	Inner Mitochondrial Membrane	Mitocarta3.0
Letm1	Ubiquitylated upon MOMP	Inner Mitochondrial Membrane	Mitocarta3.0
Maoa	Ubiquitylated upon MOMP	Outer Mitochondrial Membrane	Mitocarta3.0
Marc2	Ubiquitylated upon MOMP	Outer Mitochondrial Membrane	Mitocarta3.0
March5	Ubiquitylated upon MOMP	Outer Mitochondrial Membrane	Mitocarta3.0
Mavs	Ubiquitylated upon MOMP	Outer Mitochondrial Membrane	Mitocarta3.0
Mcl1	Ubiquitylated upon MOMP	Outer Mitochondrial Membrane	Mitocarta3.0
Mdh2	Ubiquitylated upon MOMP	Mitochondrial matrix	Mitocarta3.0
Mff	Ubiquitylated upon MOMP	Outer Mitochondrial Membrane	Mitocarta3.0
Mfn1	Ubiquitylated upon MOMP	Outer Mitochondrial Membrane	Mitocarta3.0
Mfn2	Ubiquitylated upon MOMP	Outer Mitochondrial Membrane	Mitocarta3.0
Mgst1	Ubiquitylated upon MOMP	Unknown mitochondrial localisation	Mitocarta3.0
Micu1	Ubiquitylated upon MOMP	Inner Mitochondrial Membrane	Mitocarta3.0
Micu2	Ubiquitylated upon MOMP	Inner Mitochondrial Membrane	Mitocarta3.0
Mp68	Ubiquitylated upon MOMP	Inner Mitochondrial Membrane	Mitocarta3.0
Mpc1	Ubiquitylated upon MOMP	Inner Mitochondrial Membrane	Mitocarta3.0
Mtch1	Ubiquitylated upon MOMP	Outer Mitochondrial Membrane	Mitocarta3.0
Mtch2	Ubiquitylated upon MOMP	Outer Mitochondrial Membrane	Mitocarta3.0
Mtco2	Ubiquitylated upon MOMP	Unknown mitochondrial localisation	Uniprot
Mtfr1l	Ubiquitylated upon MOMP	Unknown mitochondrial localisation	Mitocarta3.0
Mtx1	Ubiquitylated upon MOMP	Outer Mitochondrial Membrane	Mitocarta3.0
Mtx2	Ubiquitylated upon MOMP	Outer Mitochondrial Membrane	Mitocarta3.0
Mul1	Ubiquitylated upon MOMP	Outer Mitochondrial Membrane	Mitocarta3.0

Ndufa3	Ubiquitylated upon MOMP	Inner Mitochondrial Membrane	Mitocarta3.0
Ndufa4	Ubiquitylated upon MOMP	Inner Mitochondrial Membrane	Mitocarta3.0
Ndufa8	Ubiquitylated upon MOMP	Inner Mitochondrial Membrane	Mitocarta3.0
Ndufb1	Ubiquitylated upon MOMP	Inner Mitochondrial Membrane	Mitocarta3.0
Ndufb10	Ubiquitylated upon MOMP	Inner Mitochondrial Membrane	Mitocarta3.0
Ndufb5	Ubiquitylated upon MOMP	Inner Mitochondrial Membrane	Mitocarta3.0
Ndufc2	Ubiquitylated upon MOMP	Inner Mitochondrial Membrane	Mitocarta3.0
Ndufs5	Ubiquitylated upon MOMP	Inner Mitochondrial Membrane	Mitocarta3.0
Ociad1	Ubiquitylated upon MOMP	Outer Mitochondrial Membrane	Mitocarta3.0
Parl	Ubiquitylated upon MOMP	Inner Mitochondrial Membrane	Mitocarta3.0
Pet117	Ubiquitylated upon MOMP	Inner Mitochondrial Membrane	Mitocarta3.0
Pgam5	Ubiquitylated upon MOMP	Outer Mitochondrial Membrane	Mitocarta3.0
Phb	Ubiquitylated upon MOMP	Inner Mitochondrial Membrane	Mitocarta3.0
Phb2	Ubiquitylated upon MOMP	Inner Mitochondrial Membrane	Mitocarta3.0
Plgrkt	Ubiquitylated upon MOMP	Unknown mitochondrial localisation	Mitocarta3.0
Ppif	Ubiquitylated upon MOMP	Mitochondrial matrix	Mitocarta3.0
Prdx3	Ubiquitylated upon MOMP	Mitochondrial matrix	Mitocarta3.0
Ptges2	Ubiquitylated upon MOMP	Inner Mitochondrial Membrane	Mitocarta3.0
Ptrh2	Ubiquitylated upon MOMP	Outer Mitochondrial Membrane	Mitocarta3.0
Rdh13	Ubiquitylated upon MOMP	Inner Mitochondrial Membrane	Mitocarta3.0
Rhot1	Ubiquitylated upon MOMP	Outer Mitochondrial Membrane	Mitocarta3.0
Rhot2	Ubiquitylated upon MOMP	Outer Mitochondrial Membrane	Mitocarta3.0
Samm50	Ubiquitylated upon MOMP	Outer Mitochondrial Membrane	Mitocarta3.0
Sco1	Ubiquitylated upon MOMP	Inner Mitochondrial Membrane	Mitocarta3.0
Scp2	Ubiquitylated upon MOMP	Inner Mitochondrial Membrane	Mitocarta3.0
Sdha	Ubiquitylated upon MOMP	Inner Mitochondrial Membrane	Mitocarta3.0
Sfxn1	Ubiquitylated upon MOMP	Inner Mitochondrial Membrane	Mitocarta3.0
Sfxn2	Ubiquitylated upon MOMP	Inner Mitochondrial Membrane	Mitocarta3.0
Shmt2	Ubiquitylated upon MOMP	Mitochondrial matrix	Mitocarta3.0
Slc25a10	Ubiquitylated upon MOMP	Inner Mitochondrial Membrane	Mitocarta3.0
Slc25a12	Ubiquitylated upon MOMP	Inner Mitochondrial Membrane	Mitocarta3.0
Slc25a13	Ubiquitylated upon MOMP	Inner Mitochondrial Membrane	Mitocarta3.0
Slc25a20	Ubiquitylated upon MOMP	Inner Mitochondrial Membrane	Mitocarta3.0
Slc25a22	Ubiquitylated upon MOMP	Inner Mitochondrial Membrane	Mitocarta3.0
Slc25a24	Ubiquitylated upon MOMP	Inner Mitochondrial Membrane	Mitocarta3.0
Slc25a25	Ubiquitylated upon MOMP	Inner Mitochondrial Membrane	Mitocarta3.0
Slc25a3	Ubiquitylated upon MOMP	Inner Mitochondrial Membrane	Mitocarta3.0
Slc25a4	Ubiquitylated upon MOMP	Inner Mitochondrial Membrane	Mitocarta3.0
Slc25a40	Ubiquitylated upon MOMP	Inner Mitochondrial Membrane	Mitocarta3.0
Slc25a46	Ubiquitylated upon MOMP	Outer Mitochondrial Membrane	Mitocarta3.0
Slc25a5	Ubiquitylated upon MOMP	Inner Mitochondrial Membrane	Mitocarta3.0
Smim37	Ubiquitylated upon MOMP	Unknown mitochondrial localisation	Uniprot
Stmp1	Ubiquitylated upon MOMP	Unknown mitochondrial localisation	Uniprot
Surf1	Ubiquitylated upon MOMP	Inner Mitochondrial Membrane	Mitocarta3.0
Synj2bp	Ubiquitylated upon MOMP	Outer Mitochondrial Membrane	Mitocarta3.0
Tdrkh	Ubiquitylated upon MOMP	Unknown mitochondrial localisation	Mitocarta3.0
TIMM10	Ubiquitylated upon MOMP	Inner Mitochondrial Membrane	Mitocarta3.0
TIMM13	Ubiquitylated upon MOMP	Inner Mitochondrial Membrane	Mitocarta3.0

TIMM21	Ubiquitylated upon MOMP	Inner Mitochondrial Membrane	Mitocarta3.0
TIMM22	Ubiquitylated upon MOMP	Inner Mitochondrial Membrane	Mitocarta3.0
TIMM23	Ubiquitylated upon MOMP	Inner Mitochondrial Membrane	Mitocarta3.0
TIMM50	Ubiquitylated upon MOMP	Inner Mitochondrial Membrane	Mitocarta3.0
TIMM8a1	Ubiquitylated upon MOMP	Inner Mitochondrial Membrane	Mitocarta3.0
TIMM8b	Ubiquitylated upon MOMP	Inner Mitochondrial Membrane	Mitocarta3.0
TIMM9	Ubiquitylated upon MOMP	Inner Mitochondrial Membrane	Mitocarta3.0
Tmem126a	Ubiquitylated upon MOMP	Inner Mitochondrial Membrane	Mitocarta3.0
Tmem14c	Ubiquitylated upon MOMP	Inner Mitochondrial Membrane	Mitocarta3.0
TOMM20	Ubiquitylated upon MOMP	Outer Mitochondrial Membrane	Mitocarta3.0
TOMM22	Ubiquitylated upon MOMP	Outer Mitochondrial Membrane	Mitocarta3.0
TOMM40	Ubiquitylated upon MOMP	Outer Mitochondrial Membrane	Mitocarta3.0
TOMM5	Ubiquitylated upon MOMP	Outer Mitochondrial Membrane	Mitocarta3.0
TOMM7	Ubiquitylated upon MOMP	Outer Mitochondrial Membrane	Mitocarta3.0
TOMM70a	Ubiquitylated upon MOMP	Outer Mitochondrial Membrane	Mitocarta3.0
Trabd	Ubiquitylated upon MOMP	Unknown mitochondrial localisation	Proteinatlas
Tspo	Ubiquitylated upon MOMP	Outer Mitochondrial Membrane	Mitocarta3.0
Uqcc3	Ubiquitylated upon MOMP	Inner Mitochondrial Membrane	Mitocarta3.0
Uqcrc2	Ubiquitylated upon MOMP	Inner Mitochondrial Membrane	Mitocarta3.0
Uqcrfs1	Ubiquitylated upon MOMP	Inner Mitochondrial Membrane	Mitocarta3.0
Uqcrh	Ubiquitylated upon MOMP	Inner Mitochondrial Membrane	Mitocarta3.0
Uqcrq	Ubiquitylated upon MOMP	Inner Mitochondrial Membrane	Mitocarta3.0
Usp30	Ubiquitylated upon MOMP	Outer Mitochondrial Membrane	Mitocarta3.0
Vdac1	Ubiquitylated upon MOMP	Outer Mitochondrial Membrane	Mitocarta3.0
Vdac2	Ubiquitylated upon MOMP	Outer Mitochondrial Membrane	Mitocarta3.0
Vdac3	Ubiquitylated upon MOMP	Outer Mitochondrial Membrane	Mitocarta3.0
Xrcc6bp1	Ubiquitylated upon MOMP	Mitochondrial Intermembrane Space	Mitocarta3.0
Yme1l1	Ubiquitylated upon MOMP	Inner Mitochondrial Membrane	Mitocarta3.0